HHS Public Access

Author manuscript

Concepts Magn Reson Part A Bridg Educ Res. Author manuscript; available in PMC 2015 November 01.

Published in final edited form as:

Concepts Magn Reson Part A Bridg Educ Res. 2014 November ; 43(6): 237–266. doi:10.1002/cmr.a.21321.

Fetal MRI: A Technical Update with Educational Aspirations

Ali Gholipour, PhD[1], **Judith A. Estroff, MD**[1], **Carol E. Barnewolt, MD**[1], **Richard L. Robertson, MD**[1], **P. Ellen Grant, MD**[1], **Borjan Gagoski, PhD**[1], **Simon K. Warfield, PhD**[1], **Onur Afacan, PhD**[1], **Susan A. Connolly, MD**[1], **Jeffrey J. Neil, MD**[1], **Adam Wolfberg, MD**[2], and **Robert V. Mulkern, PhD**[1]

[1]Department of Radiology, Boston Children's Hospital, Boston, Massachusetts, USA

[2]Boston Maternal Fetal Medicine, Boston, Massachusetts, USA

Abstract

Fetal magnetic resonance imaging (MRI) examinations have become well-established procedures at many institutions and can serve as useful adjuncts to ultrasound (US) exams when diagnostic doubts remain after US. Due to fetal motion, however, fetal MRI exams are challenging and require the MR scanner to be used in a somewhat different mode than that employed for more routine clinical studies. Herein we review the techniques most commonly used, and those that are available, for fetal MRI with an emphasis on the physics of the techniques and how to deploy them to improve success rates for fetal MRI exams. By far the most common technique employed is single-shot T2-weighted imaging due to its excellent tissue contrast and relative immunity to fetal motion. Despite the significant challenges involved, however, many of the other techniques commonly employed in conventional neuro- and body MRI such as T1 and T2*-weighted imaging, diffusion and perfusion weighted imaging, as well as spectroscopic methods remain of interest for fetal MR applications. An effort to understand the strengths and limitations of these basic methods within the context of fetal MRI is made in order to optimize their use and facilitate implementation of technical improvements for the further development of fetal MR imaging, both in acquisition and post-processing strategies.

Keywords

Fetal MRI; Technical update; Review

1. Introduction

Those of us who have had the pleasure of observing the development of clinical MRI from its inception in the mid-1980's through current times can't help but note the difference between how exams are performed now vs. then. In the good old days, radiologists would commonly be standing shoulder-to-shoulder with the technologists running the scans, back-seat driving for better or worse. Today, scanning technologists rarely have face-to-face encounters with reading radiologists who may, or may not, communicate with technologists from remote satellite stations during individual MR examinations. Perhaps this is why it is so refreshing to enter the MR console room and witness a fetal MRI examination being performed. It is as if one has been transported back-to-the-past! There is the radiologist, not just back seat driving but, as often as not, actually running the scans! An interactive, fervent,

process is occurring wherein planes are being proscribed on the fly from the preceding scan to try to target suspect anatomy before the fetus twists and turns away from view. In this regard, fetal MRI involves using the scanners differently than in most other applications, more in the “real-time” mode commonly associated with ultrasound procedures. It is indeed a testament to the steady development of hardware and software over the last 30 years that fetal MRI has been able to become a well-established, if challenging, endeavor.

The cost and complexity of MRI compared to ultrasound (US) have largely relegated fetal MRI to that of an adjunct modality which is, however, deemed useful when diagnostic questions remain after US (1–9). Clinical indications for fetal MRI run the gamut from central nervous system disorders (1, 6, 10–20), abdominal, pulmonary, and musculoskeletal concerns (21–23), and evaluation of maternal organs critical for fetal development and delivery such as the placenta (24–28) and cervix (29–32). The field has achieved a maturity that has endowed it with excellent review articles regarding multiple clinical findings and uses to date (5, 14, 15, 33–39). Digital atlases of the fetal brain based on fetal MRI have been generated (40–43) and work on MRI based biometric fetal growth markers continues to move forward (44–48).

It is of interest to note that the majority of information available from fetal MRI examinations to date has been extracted using single-shot T2-weighted (SST2W) imaging. We contend that with careful attention to detail, and with some obvious restrictions, it is possible to obtain T1-weighted images, T2*-weighted images, T2/T1-weighted cinematographic images, diffusion weighted images and their associated diffusion parameter maps, spectroscopic data, and even arterial spin labeled images, all tools that have yet to be fully exploited in fetal MRI. In this work we will discuss in some detail the MR methodology, current and potential, for use in fetal MRI examinations. Technical issues arising in the use of different methods in the context of fetal MRI will be addressed and observations on what is currently lacking or inadequate as a consequence of the special challenges encountered will be made. Some developments being taken to improve the methodology, including motion correction and compensation schemes as well as post-processing approaches to provide more robust anatomical and/or functional information, are examined.

2. Technique Review

Before launching into detailed discussions of each technique applicable to fetal MRI, it may be useful to state a “golden rule”, proffered by a fetal imaging radiologist and contributing coauthor, which should be considered quite seriously when designing each protocol. Since the major challenge is to capture quiescent periods of fetal motion, one should try to keep each scan to ~ 25 s or less, have a look at the images generated, reposition the slices and/or change technique, and scan again. Avoiding the scanner specific “autoprescans” (49) for repeat scans with the same sequence is strongly recommended, as these will unnecessarily waste examination time with little or no benefit in image quality (one autoprescan per technique). An allotted 45 minute slot will be filled up quite efficiently with this approach, and the probability of a successful diagnostic outcome will be increased. Of course this ~ 25 s “golden rule” will affect the types of sequences which can be run, the parameters

associated with such sequences and the volume coverage, or number of slices, interrogated per scan. With this in mind we begin our technical review of the methods applicable to fetal MRI.

a. Single-shot T2-weighted Imaging: The front-line fetal imaging technique

Fetal motion is irregular and unpredictable, rendering images acquired with conventional, multi-slice, two-dimensional (2D) scanning techniques that last several minutes, diagnostically useless. Towards the latter stages of pregnancy, engagement of the head within the uterus can significantly reduce fetal motion, though this can hardly be predicted beforehand and is of limited value for fetal imaging performed in earlier stages of pregnancy. Therefore, barring pharmacologic interventions such as fetal paralysis obtained with neuromuscular blockers as deployed in the early 90's (50–53), the need for some sort of "snapshot" imaging to avoid image degradation from fetal motion has been obvious from the earliest days of fetal MRI. Indeed some of the very first echo planar imaging (EPI) methods, based upon multiple gradient echo trains, were applied to study the fetus (54–57). By the mid-nineties, scanner hardware and software development had proceeded to the point where a single-shot T2-weighted (SST2W) imaging method based on RF spin echoes rather than gradient echoes became available, and it was quickly realized that this approach could be harnessed for the best anatomical evaluation of the fetus in utero (1–4). The field of fetal imaging has since been dominated by the use of this SST2W imaging. For example, a fairly recent fetal brain MRI review article by Glenn (20) displayed 25 fetal brain images, 23 of which were obtained with SST2W imaging with tissue contrast largely identical to that found in conventional T2-weighted brain scans acquired more slowly using multiple "shots". Similarly, in a review of tumors encountered in the fetal body (9), the MR images dispersed among the figures contained 12 SST2W images, 2 T1-weighted gradient echo images and one steady state free precession (SSFP) image with a T2/T1 type of contrast (vide infra). A perusal of the bulk of clinically oriented fetal MRI articles and reports published in the last 15 years yields similar results with an overwhelming display of SST2W fetal images to illustrate sundry anatomical and pathological findings. Though clearly the front-line technique for fetal imaging, it is of interest to note that SST2W imaging has found limited clinical application elsewhere, e.g. cholangiography where very heavily T2-weighted imaging is deemed diagnostic (58), and rapid imaging of nonsedated neonates and children for example to monitor ventricular size in infants with shunt catheters.

Reasons for the popularity of SST2W imaging for fetal imaging studies are fairly simple – the ability to largely "freeze" motion and to supply excellent T2-contrast. Reasons for its unpopularity for most other applications are equally simple to understand – relatively low spatial resolution and the limitation to T2-contrast governed by point spread function considerations and the desire to avoid image blurring. These features warrant some discussion of the underlying physical principles to understand the relative strengths and weaknesses and allow thought for potential improvements. The currently available SST2W sequences go by a number of vendor specific names: Single-Shot Fast Spin Echo (SSFSE) - General Electric Medical systems; HAlf-fourier Single-shot Turbo spin Echo (HASTE) – Siemens; Single-Shot half-Fourier Turbo Spin Echo (SShTSE) – Philips; Rapid Acquisition with Relaxation Enhancement (RARE) – Bruker Instruments. The vendor free acronym we

employ, SST2W, is employed herein because it succinctly describes the most important attributes of the method which are its single-shot (SS) nature (minimizing intra-scan motion artifact and T1-weighting), and its relatively pure T2-weighting, not T2*, T1 or T2/T1, which best describes its tissue contrast. Some basic facts about SST2W sequence are the following; I) A single slice selective excitation pulse is followed by a series of slice selective refocusing pulses, each of which causes a "spin-echo" to be formed whose individual duration is on the order of 2 to 3 ms. II) Each spin echo is "read out" with appropriate digitization, e.g. very high bandwidth readouts during the frequency encoding which is preceded and followed by appropriate "wind" and "rewind" phase encode gradients such that each echo forms a line in "k-space" from which, following acquisition of all echoes, an image is generated using 2D Fourier transformation. III) The effective echo time (ETE) which determines the degree of T2 contrast weighting is governed by the specific ordering of the phase encodes with respect to the individual spin-echo times such that the specific echo times used for the low order phase encode lines determine the ETE associated with the T2 contrast (59–64). With several caveats discussed below, the signal *S* in SST2W imaging is given by

$$S = Cpe^{-\mathrm{ETE}.R_2} \quad (1)$$

where *C* is a proportionality constant associated with receiver coil sensitivity and voxel size, *p* is the spin density, and $R_2 = {}^{1}\!/_{\mathrm{T2}}$ is the irreversible transverse relaxation rate, in s^{-1}, a rate distinct from the so-called reversible transverse relaxation rate R_2' which comes into play in gradient echo imaging as discussed further below.

Since the fetus and its organs tend to be small and the pregnant mothers' abdomens large, it is difficult to use otherwise desirable small fields-of-view (FOV's) and avoid wrap-around artifact, particularly along the phase encode direction. As a consequence, fairly large FOV's are usually employed (generally > 30 cm) with fairly large matrix sizes (256 × 256 or larger) required to attain reasonable in-plane spatial resolutions (~1×1 to 2×2 mm^2) for fetal organ imaging, but smaller FOVs (e.g. 24–28 cm) may be used in fetal brain imaging when possible. An SST2W imaging sequence would then theoretically have to have at least 256 echoes to do the job. With modern hardware, echo spacings on the order of 3 to 5 ms are available which make 256 echo train lengths quite long compared to, say, fetal brain parenchyma T2 values which, extrapolating from newborn data (65), can be greater than 200 ms. Thus it may be anticipated that T2 decay would severely deteriorate signals from the later echoes within the SST2W echo trains and so degrade image quality. As a consequence, the vendor supplied SST2W sequences tend to utilize half-Fourier acquisitions in which only slightly more than half of the k-space lines are acquired. The remaining k-space lines are generated using idealized Hermitian conjugate symmetry of k-space with some phase corrections supplied by ~ 10 % oversampling of the idealized ½ k-space. The result is echo trains lasting on the order of 500ms, which generate k-space datasets suitable for image reconstruction, largely freezing intra-scan motion (66).

Given the constraints discussed above, typical SST2W images have 1×1 to 2×2 mm^2 in-plane spatial resolutions with slice thicknesses between 2 and 4 mm. Furthermore, when

proscribing multiple slices or a “stack” of slices, sequential slice acquisitions with minimum delays between successive slice samplings will minimize the time required to cover a selected volume. This is critical to avoid the effects of inter-slice fetal motion during the full volume interrogation where scans lasting more than 20 to 30 seconds often lead to poor results. As an example, proscribing 26, 4-mm thick slices each sampled in ~ 700 ms will yield a total scan time of only ~ 18 s and provide coverage of over 10 cm of fetus in the slice selection direction. The effective TR with respect to spin-lattice relaxation time T1 differences is infinity, since no pulses have interrogated any slice of interest prior to the excitation pulse. Though “cramming” as many slices as possible into a specified period of time during which one hopes for little fetal motion (say a 25 s rule) is obviously beneficial, some deleterious effects do occur which can be avoided with a judicious delay between slice samplings. For instance, amniotic fluid has a long T1 and is often also in a state of convective motion. Thus amniotic fluid saturated in one slice can find itself in an adjacent slice during the latter slice’s interrogation, demonstrating signal loss and spoiling the pristine quality of an image in which a fetus is viewed within a bright bath of amniotic fluid.

Another, perhaps more subtle effect is that of magnetization transfer (MT) when performing multi-slice acquisitions (67). Namely, sampling adjacent slices applies off-resonance irradiation to the other slices, resulting in a reduced signal in the latter from tissues harboring macromolecules. Figure 1 compares an SST2W image from a “crammed” TR multi-slice acquisition with a single slice acquisition of the same slice, barring some minor fetal/maternal displacement between the two acquisitions. The images demonstrate these two deleterious, if not devastating, effects on image quality. Both the flow of saturated amniotic fluid or MT effects can clearly be reduced by allowing for delays between sequential slice sampling, though this must be weighed against the effects of prolonging the overall scan time needed for a stack of slices, breaking the “golden rule” and so inviting potentially more serious image degradation from inter-slice fetal motion. The latter can obliterate the careful slice proscriptions designed to select specific anatomical planes for desired displays of, for example, fetal brain, lung, or palate. To minimize slice crosstalk and spin history artifacts sequence may be performed in an interleaved manner, typically with 2 concatenations. When the slice distance is too short, e.g. with 2 mm slice thickness and no slice gap, 3 or even 4 concatenations may be used to minimize possible effect of motion-induced spin history artifacts.

A further, oft unconsidered default parameter in SST2W imaging is the flip angle of the refocusing pulses which, in the purest form of multi-echo imaging is set to 180°. On close examination of the default settings of refocusing flip angles for the SST2W sequences provided by the standard vendors, however, values considerably less than 180° and in the 120° to 150° range are found. This is justified for at least two reasons, the first being that it is a simple way to reduce the amount of power transmitted to the mother and child, so-called specific absorption rate (SAR) considerations (68–74). The second is that stimulated echoes will arise further out in the echo train which have mixed T1 and T2 relaxation properties (75–78), allowing for more signal to become available at later echo times than would have arisen from the primary echoes generated with perfect 180° refocusing pulses. We have also noted that for at least one vendor (GE), reducing the flip angle results in shorter RF pulse durations which results in reduced echo spacing and hence less overall T2 decay throughout

the echo train, potentially improving image quality. An example of the effects on image quality and typical tissue signal intensities as one varies the RF refocusing flip angles between 110° and 150° are shown in Figure 2 and Figure 3, respectively. The improvements in signal with larger flip angles are not very dramatic, making the use of the lower flip angles prudent from a power absorption perspective. Indeed, since SST2W sequences are associated with some of the highest SAR values of all imaging sequences, such considerations are important and will become even more relevant as 3T scanners become employed for fetal imaging more often, as they invariably will.

The above discussions point towards some potential improvements in SST2W imaging. For example, the use of variable refocusing flip angles along the echo train, currently employed in long echo train 3D FSE acquisitions (79) might be gainfully applied to the SST2W 2D echo trains in the future for improved image quality and reduced SAR values as will be required at higher field strengths like 3T. Also with the advent of multi-coil arrays, multiple receiver channels and the explosion of parallel imaging reconstruction methods (80) in recent years, the echo trains associated with SST2W imaging may be further reduced from their current values while maintaining the requisite number of phase encoding steps needed for high spatial resolution. This would alleviate some of the blurring artifact associated with T2 decay at the expense of some SNR, an approach that may prove particularly useful in achieving shorter effective echo times required for either Proton Density (PD) or T1-weighted contrasts with single-shot RF echo trains. Alternatively, parallel imaging approaches may be used to increase spatial resolution along the phase encode dimension by utilizing echo train lengths currently employed. Improving spatial resolution may also be considered by limiting the field-of-view with inner volume methods (81, 82) to avoid aliasing artifacts that hamper smaller FOV imaging. The degree to which such methods can be gainfully exploited remains to be examined.

To summarize, default settings of the common vendor supplied SST2W sequences include half-Fourier acquisitions with RF refocusing flip angles in the 120° to 150° range. As currently implemented, they are well-suited for generating, in approximately 500 ms or less, a T2-weighted image largely free of intra-scan motion artifacts, in-plane spatial resolutions of 1×1 to 2×2 mm^2 and slice thicknesses from 2 to 4 mm. At 1.5 T, where the bulk of fetal imaging with SST2W imaging has been performed, few complaints regarding SST2W fetal imaging are justified, apart from perhaps the low spatial resolution. Future efforts to improve SST2W imaging may take the form of more careful consideration of RF refocusing flip angle variations as well as advanced k-space sampling strategies which go above and beyond simple half-Fourier methods. Certainly some of these considerations will be needed as 3T scanners become accessible for fetal imaging and SAR issues become more prominent along with potentially shorter T2 relaxation times.

b. Single-shot T1-weighted (SST1W) imaging with inversion recovery methods

From a clinical perspective, it may be argued that T1-weighted imaging is often less sensitive to pathology than T2-weighted imaging, though of course the generality of this statement cannot be used to deny the valuable anatomical and contrast specific diagnostic uses of the former. The single-shot readouts with long spin-echo trains used so successfully

for T2-weighted fetal imaging can also be used for single-shot T1-weighted (SST1W) imaging with two fairly simple modifications that are available on most scanners. First, a slice-selective inversion pulse is applied at a specified inversion time (TI) prior to each slice selective excitation pulse of the SST1W echo train which serves to introduce the T1-weighting. Second, the ETE of the echo train is lowered to minimize the T2-weighting by, for example, using centric phase encode reordering in which the smallest phase encodes are acquired from the earliest echoes (83). The signal intensity from such a sequence may be approximated with the following equation:

$$S = C\left|1 - e^{-\mathrm{TI}.R_1}\right| e^{-\mathrm{ETE}.R_2} \quad (2)$$

where $R_1 = {}^{1}\!/_{\mathrm{T1}}$ is the longitudinal, or spin-lattice relaxation rate (in s^{-1}) and the other terms have been previously defined. The absolute value sign in Equation 2 reflects the common practice of magnitude reconstruction from k-space data. Though phase reconstruction methods would preserve the sign of the T1-weighting term and double the dynamic range of this weighting, such reconstructions are generally challenging if worthy of further consideration in the context of fetal imaging (83), particularly as magnitude reconstruction complicates T1 interpretation as two tissues with widely disparate T1 values may appear with the same signal intensity. Figure 4 is a typical SST1W fetal image acquired using this approach in which we utilized a TI of 2 s and an ETE of 30 ms, chosen so that fat is bright, brain parenchyma intermediate, and CSF dark, as expected for classic T1-weighted imaging. Figure 5 shows simulations based on Equation 2 for these tissues which provided a rationale for this choice of a 2 s TI given typical longitudinal relaxation rates, provided in the figure legend, for these tissues. Figure 5 also demonstrates how, due to magnitude reconstruction, some TI values can lead to similar signal intensities from tissues with different T1 values, a feature that might be avoided using phase reconstruction methods. We note that Malamateniou et al. (83) advocated use of a shorter TI of 400 ms, followed by inversion of the magnitude signal intensity, for display in efforts to generate some grey/white matter contrast in fetal brains, though we find our TI of 2000 ms to be suitable as well for basic T1-weighting which separates fat (bright) from brain (isointense) from CSF (dark).

The use of an inversion pulse and inversion time TI invariably reduces signal-to-noise from all tissues in inversion recovery SST1W. A further image quality detractor is the lowering of the ETE towards the beginning of the echo train which reduces T2 effects but also means that higher phase encoding steps have T2-diminished signal intensities. This results in blurry images or, in more technical terms, a degraded point spread function (84). Steps towards ameliorating this problem may be made in the future by considering variable flip angle refocusing trains as discussed above, and by using parallel imaging schemes to reduce the length of the echo trains without compromising spatial resolution albeit with reduced SNR. Phase reconstruction and more efficient interleaving of slice inversions and slice interrogations to reduce overall scan times, as performed in modern multi-shot fluid attenuated inversion recovery (FLAIR) sequences, are two further possibilities that would improve SST1W fetal imaging which, despite current efforts, remains less satisfying than SST2W fetal imaging.

c. Gradient Echo Imaging: Spoiled and Unspoiled sequences for T1, T2* and cinematographic T2/T1 weightings

Like children, gradient echo imaging sequences come in at least two flavors - spoiled and unspoiled – with both having their charms. The nomenclature among the vendors is, of course, varied and confusing and for the purposes of this discussion we will restrict ourselves to calling spoiled versions Spoiled GRadient echo (SPGR) sequences to emphasize the "spoiling" aspect as explained below. For the unspoiled versions we will use an original term (85) Steady State Free Precession (SSFP) sequences to emphasize the "free precession" aspect in which the inherent intra-voxel frequency effect is not forgotten due to imaging gradients and/or RF phase cycling. Because of this however, the very characterization of SSFP as a "gradient echo" sequence from a tissue contrast perspective as opposed to the frequency encoding sequence diagram perspective is questionable as spin-echo like behavior is also involved in tissue contrast (86), albeit in a complicated fashion as discussed further below.

Thus we first turn our attention to the spoiled versions. The act of "spoiling" refers to a technical feature within the pulse sequence such that immediately prior to each RF pulse no net transverse magnetization components exist - they have been "spoiled". For short TR periods, the spoiling is performed typically with a combination of "spoiler" gradients and by varying the phases of the RF pulses used to solicit signals from the sample (87). For longer TR periods (TR $\gg$ T2* where T2* is discussed in detail below) the long delay following echo collection largely insures that T2* decay has substantially diminished the transverse components. All or some of these steps are taken to insure that, as much as possible, there is a total lack of transverse magnetization prior to each RF pulse. In this manner, spoiled gradient echo signals collected after RF pulses reflect only the longitudinal magnetization that was available prior to the pulse. This steady state longitudinal magnetization in turn depends upon the T1 of the tissue in question, the flip angle of the RF pulses employed and the repetition time TR between RF pulses. Further tissue contrast is determined by the echo time TE selected for signal formation via read gradient reversal, not RF refocusing, and determines the degree of T2* weighting, not T2-weighting, in spoiled gradient echo imaging. Thus an SPGR sequence consists simply of a string of RF pulses with flip angle α, and varying RF phases, separated by a repetition time TR with each readout pulse followed by a gradient echo readout at time TE which is then followed by spoiler gradients. The equation governing the signal from tissue in SPGR is:

$$S = C[1-e^{-\mathrm{TR}.R_2}]\sin\alpha.e^{-\mathrm{TE}.R_2^*} \Big/ [1-\cos\alpha.e^{-\mathrm{TR}.R_1}] \quad (3)$$

where $R_2^* = 1/T2^*$ is a transverse relaxation rate that is the combination of both reversible and irreversible transverse relaxation rates R_2 and R_2', respectively with $R_2^* = R_2 + R_2'$. If these brief but factual statements regarding transverse relaxation rates are confusing, the reader is directed towards the more comprehensive treatment by Ma and Wehrli regarding reversible vs. irreversible transverse relaxation processes (88). For our purposes, it is sufficient to know that some transverse relaxation, or dephasing in the transverse plane, is caused by "irreversible" processes such as the microscopic, time-varying, magnetic dipole-dipole interactions between spins. This "irreversible" T2 decay is governed by the rate

constant R_2 and is impervious to the application of RF pulses. On the other hand, some processes, like static spin dephasing due to inherent frequency distribution within a voxel is largely "reversible" in the sense that an RF pulse results in a rephasing of the spins at a specific time after the pulse. These reversible processes are to be associated with the relaxation rate R_2' which is actually a measure of the half-width of the inherent distribution of frequencies within a voxel, though only in the case of a Lorentzian distribution does a specific mathematical relationship between the half-width and R_2' exist (88, 89). In a pure spin echo or multiple spin echo sequence with 180° refocusing pulses, full rephasing of reversible relaxation largely occurs so that the decay is governed by irreversible T2 decay alone. For spoiled gradient echo sequences, the rephasing of the spins is not due to refocusing RF pulses but rather due to a gradient reversal with the result that both reversible and irreversible transverse relaxation mechanisms contribute to the decay whose rate constant is then governed by $R_2^* = R_2 + R_2'$. The difference between T2 and T2* weighting is key in such applications as blood product detection where reversible dephasing caused by susceptibility effects associated with iron containing blood products result in substantial T2* dephasing which will not be so obvious in T2-weighting. It is also of interest to note that newborns, and by extrapolation fetuses, have much longer brain parenchyma T2* values than adults (90) so that longer TE's may be necessary to appropriately weight fetal T2* SPGR sequences compared to those used in adults. Figure 6 is an excellent example of T2* weighted fetal imaging with an SPGR sequence in which a hypointense, periventricular lesion stands out as a suspected blood product resulting from a hemorrhagic process. This lesion was not appreciated in any of the other sequences applied in this examination (see Figure caption).

Golden rule scan time considerations applied to T2*-weighted SPGR fetal imaging will generally require the operator to severely limit the number of slices per scan. For example, the image shown in Figure 6 utilized a 150 ms TR, a 25 ms TE and a 20° flip angle (FA) with each echo being read in approximately 8 ms. With the spoiling following each echo acquisition, only 4 slices could be interrogated within the TR interval and with 128 phase encodes, the entire scan for the four slices took approximately 20 s. Also, a key difference from the SST2W imaging is that data is being collected in an interleaved manner for all the slices throughout the entire scan time, making the overall process much more susceptible to motion degradation effects. Thus it is prudent to limit the number of slices so that short scans are performed, images examined, and new slices proscribed or repeated as appropriate, until the entire anatomy of interest has been properly interrogated. Again, avoiding pre-scans for all acquisitions after the first is recommended to increase the probability of diagnostic success. The combination of sequence parameters we have settled on for T2*-weighted imaging appears to provide the necessary tissue contrast, SNR and spatial resolution for the primary application, detecting blood-products, while adhering to the golden rule with the major drawback being the reduced volume coverage per scan.

It is also possible to obtain T1-weighting with SPGR sequences by simply increasing the flip angle and reducing the echo time to minimum values. Malamateniou et al. (83), for example, compared such T1-weighted SPGR methods, acquiring 12 slices in 17 s with a 142 ms TR and 6 ms TE periods for comparison with their inversion recovery SST1W method discussed above. They found the former lacking in image quality with increased sensitivity to motion

artifact as a consequence of the interleaved nature of the multi-slice acquisition compared to the single-shot approaches like SST1W inversion recovery.

Recent developments with 3D SPGR imaging provide another promising approach for T1-weighted fetal imaging. In particular fast 3D SPGR sequences that utilize asymmetric partial k-space sampling along with interpolation (zero filling), short TR/TE periods, and parallel imaging techniques can provide good-quality T1-weighted imaging of the fetus. Such 3D SPGR sequences, with vendor names like VIBE from Siemens (volumetric interpolated breath-hold examination), LAVA from GE (Liver Acquisition with Volume Acquisition – General Electric Medical systems), or THRIVE from Philips (T1-weighted High Resolution Isotropic Volume Examination), are specifically designed to achieve short total acquisition time (<30 seconds) for applications like breath-hold liver imaging (91–93), automatically adhering to the golden rule. Noise reduction filters are used to compensate for the reduction in SNR caused by partial k-space sampling. An optimized inversion pulse and a fat selective pre-pulse are used to improve image contrast and achieve uniform fat suppression. Typical parameters for a T1-weighted MRI of the fetal brain with VIBE which we use are TR/TE=3.64/1.28 ms with a flip angle of 9°. Figure 7 shows such a VIBE scan of a fetus acquired at 3T. Despite the short acquisition times, VIBE is generally more sensitive to motion than single-shot 2D methods as the 3D data is being acquired from the entire 3D volume throughout the full scan time. Thus it is prudent to apply such methods when the fetus is relatively still and also preferably with maternal breath-hold.

We now turn our attention to the “unspoiled” family of gradient echo sequences with vendor names like FIESTA (fast imaging employing steady-state acquisition), true-FISP and b-SSFP where the b stands for “balanced” or compensated imaging gradients, the means by which their effects on the natural “free precession” of the spin system is removed. The balancing act means that for every gradient applied for the image formation process, a counter-gradient is also applied so that the spin system has no memory (or as little as possible) of the imaging gradients prior to witnessing each RF pulse. In this manner, and in distinction with the spoiled approach, transverse magnetization components are retained and available for manipulation by the RF pulse. This difference between spoiled and unspoiled gradient echo imaging, the lack or non-lack of transverse magnetization prior to each RF pulse, may seem like a small, technical detail. In fact, however, it has a tremendous impact in terms of, SNR, SNR/unit time, tissue contrast, and artifact. Figure 8 shows simulation results of magnitude signal vs. flip angle for a tissue like fetal brain parenchyma that exemplifies how unspoiled gradient echo imaging provides much higher SNR as compared to spoiled gradient echo sequences. As Sheffler and Lehnhardt noted in their review of the clinical applications (85), unspoiled gradient echo sequences offer “…the highest possible signal-to-noise ratio (SNR) per unit time of all known sequences.” Given this fact, it is of interest to contemplate why SSFP does not play a much larger role than it does in basic anatomical imaging, albeit it has proven extremely, indeed uniquely, useful in some specific applications. These include localizer or “scout” imaging, cardiac imaging (85, 86, 94) and some fetal imaging, including specific anatomical imaging and studies in which a selected slice, or a modest few slices, are scanned rapidly and serially with time to study fetal motion. Examples where the latter can be helpful include assessing the fetus’s ability to move its feet in anomalies like neural tube defect, and the examination of palate, pharynx,

trachea, and airways during swallowing to assess conditions like cleft palate or airway obstruction (95–97).

The reason for a lack of widespread SSFP use can be traced to its relatively poor tissue contrast compared to T2-weighted imaging, as shown by the comparison of SST2W and SSFP fetal images in Figure 9. In addition, a banding artifact is often seen in SSFP images due to the complicated off-resonance frequency dependence, as shown in the fetal image of Figure 10. Though the banding artifact has become less of a problem with modern scanners using short (~ 5 ms or less) TR periods, the intrinsic tissue contrast of SSFP continues to hinder its widespread application for high-resolution anatomic imaging. A major advantage of SSFP in the context of fetal imaging, however, its ability for rapid serial imaging of one or a few selected slices in seconds or less in which up to half of the full magnetization available from some tissues, particularly fluid in which T1 ~ T2 remains available for high SNR imaging. Attempts to perform such serial imaging with equivalent scan time SPGR sequences would practically extinguish all signal. To justify these remarks, an examination of the somewhat more complicated expressions for SSFP signal, as handed down several decades ago (98) must be examined. These expressions, though complicated, have some useful approximate forms and can be fully explored using elementary computational software available today such as Matlab.

The steady state transverse magnetization from a string of θ_x pulses separated by τ as a function of time t, from t = 0 immediately after a pulse through t = τ immediately before the next pulse, reads:

$$S=\left(\frac{c}{a}\right)\left[e^{-i\omega t}e^{-R_2 t}-e^{-i\omega(t-\tau)}e^{-R_2(t+\tau)}\right]\Big/\left[1-\frac{b}{a}\cos\omega\tau\right] \quad (4)$$

with

$$\begin{aligned} a&=1-e^{(-(R_1+2R_2)\tau)}-\cos\theta\left[e^{-R_1\tau}-e^{-2R_2\tau}\right],\\ b&=(1+\cos\theta)e^{-R_2\tau}\left[1-e^{-R_1\tau}\right],\\ c&=im_{oo}\sin\theta\left[1-e^{-R_1\tau}\right], \end{aligned} \quad (5)$$

where ω is the angular frequency of a single isochromat, m_{oo} the equilibrium magnetization (taken as unity in all further calculations), and R_1 and R_2 are the longitudinal and irreversible transverse relaxation rates, respectively. Clearly this set of relations is considerably more daunting than the signal intensity expressions for SST2W, inversion recovery SST1W and spoiled gradient sequences provide in Equations 1 to 3. Furthermore, they contain a dependence on the isochromat frequency ω that the others do not, a consequence of the “free precession” aspect in which all imaging gradients are balanced and transverse magnetization is retained prior to each RF pulse. As mentioned above, this frequency dependence is the root cause of banding artifacts that hampered SSFP in the early days when scanner gradient subsystems could not accommodate short repetition times.

Figure 11 presents simulations of SSFP signal as a function of frequency for several tissues: CSF (T1 = T2 = 3 s), fetal brain (T1 = 1 s, T2 = 0.25 s) and muscle (T1 = 1.5 s, T2 = 0.035

s). Note that the value used for fetal brain in this comparison is somewhat longer than the nominal value (65). SSFP simulation parameters for the figure were a relatively large flip angle of 75°, TE = TR/2 and TR periods of 5 ms (blue) but also a 25 ms (red) TR for comparison for the CSF tissue. Such plots show the good and the bad of SSFP, high signal even at very short TR values (good!) but huge signal losses at specific frequencies appearing at 1/TR intervals (bad!). It is indeed remarkable that in the "passbands" the signal for T1 = T2 type tissues (fluid) is as high as ½ the available magnetization practically independent of the TR and T1. With such TR values in SPGR sequences, the signal would be nearly extinguished for long T1 tissues at all flip angles. The bad part lies in the so-called transition zones where at distinct frequencies, separated by 1/TR, signal drops to nearly 0. The capability of modern scanners to utilize TR periods on the order of 5 ms vs 25 ms, where in the latter case the banding would be intolerable (Figure 11, red solid line), greatly expanded the use of SSFP towards the turn of the century. These bands are however, still visible in fetal imaging as shown in Figure 10 which was acquired with a TR of 4.5 ms, pushing the bands out towards the outer limits of the FOV and well-away from the fetus, though other, subtler, bands attributed to frequency shifts in maternal bowel and closer to the fetus may also be present (arrows). Note from Figure 11 how the signal in the passband from CSF-like tissue is the largest, followed by fetal brain parenchyma and then followed by muscle, which has quite low signal. This is completely consistent with the ratio of their T2/T1 values. Indeed a useful approximation that can be extracted from Equations 4 and 5 for passband conditions ($w\tau = \pi$), flip angle = 90° and the typical limits $R_1\tau \ll R_2\tau \ll 1$ (a fun exercise involving expanding the exponentials to first order) is a signal approximately proportional to $R_1/(R_1 + R_2)$ which, in turn is approximately ½ as R_1 approaches R_2 and is approximately equal to T_2/T_1 for $T_1 \gg T_2$, justifying the tissue contrast remarks made above. Note that the same approximation applied to the signal for SPGR sequences (Equation 3) yields a signal proportional to TR/T_1, showing how quickly signal diminishes with decreasing TR values and increasing T1 values, something that does not happen with SSFP.

We conclude that the primary difference between spoiled gradient echo sequences and unspoiled gradient echo sequences is that with the former, rapid imaging can be performed with well-controlled degrees of either T1- or T2*-weighting but with diminishing SNR as scan speed is increased. With the latter, very rapid imaging with very high SNR can be performed serially but only with a T2/T1 type of tissue contrast which, on its own might prove somewhat limited but is useful for monitoring the anatomy through fluid tissue contrast, anatomic fetal motions, and perhaps, flowing blood abnormalities. Blindly applying spoiled gradient echo sequences used for T1 or T2*-weighted imaging in general clinical applications like brain, spine or joint imaging with large volume coverage directly to fetal imaging will be disappointing due to the relatively long scan times associated with the volume coverage and spatial resolutions typically employed. Simple considerations in this regard to keep to the golden rule of 25 s scans or less and then have the scans applied multiple times can vastly improve the success rate of these fetal imaging methods.

d. Echo Planar Imaging: Diffusion Potential for Diffusion Imaging

Echo Planar Imaging (EPI) is arguably the fastest practical way of making images. The method utilizes multiple gradient echoes to acquire many lines in k-space after a single

excitation or during an RF refocused spin-echo. Using bipolar gradient readouts, sampling along the “ramps” of the gradient pulses and reading out the individual echoes with very high receiver bandwidths, 64 k-space lines or more can be acquired in 50 ms or less, making EPI images quickly indeed but also prone to low resolution, low signal-to-noise, and geometric distortion. Figure 12 shows axial and coronal EPI scans of a fetus. Due to its incredible speed, and despite its drawbacks, EPI plays an important role in applications such as diffusion imaging, perfusion imaging, cardiac imaging, and functional brain imaging. The cost of the rapid acquisition is higher susceptibility of EPI to a number of artifacts, particularly along the phase encoding direction, which can cause signal loss, ghosting, chemical shift artifacts and off-resonance effects due to magnetic field susceptibility variations and B_0 field inhomogeneities. There are ways to reduce these artifacts through pre-scan calibration and post-processing, and despite the challenges, EPI remains a unique sequence for diffusion and perfusion imaging in many applications including fetal MRI.

Diffusion imaging, in which the images are sensitized to microscopic motions of the water molecules by sandwiching a refocussing pulse with diffusion sensitization gradients (99) relies heavily on EPI for at least two reasons. The first is to minimize the effects of uninteresting bulk motion such as pulsations and involuntary movements by “snapshot” imaging and the second is that one can quickly gather images with multiple different diffusion sensitization directions to probe anisotropies in the microscopic motions of the water molecules such as the preferred directional motion along white matter tracts. In typical diffusion EPI methods, a single TR of 2 and 3 s can accommodate sampling multiple slices with a single diffusion direction and so-called b-factor, a vector representing the strength and orientation of the diffusion sensitization. For diffusion imaging, a given slice may be imaged several times with different diffusion encodings or b-factors. These images of the slice are typically combined to create maps of diffusion parameters such as apparent diffusion coefficient (ADC) and anisotropy. In the simplest scheme, a single diffusion encoding of each slice is obtained; this provides an image in which contrast is diffusion weighted, but does not permit calculation of individual parameters such as ADC or anisotropy. A minimum of three diffusion encodings (plus a reference image with no diffusion encoding) of each slice is necessary to calculate ADC. A minimum of six is necessary to make simple anisotropy maps. For more sophisticated modeling of water displacements, over 100 encodings have been acquired in some instances. Using the speed of EPI, several signal averages can be employed to increase SNR and baseline (low b-factor) and multiple high b-factor data sets of the volume can be acquired in only several minutes of scan time. In the context of fetal imaging, it is prudent to perhaps minimize the number of directions, b-factors and signal averages to keep scan times low. It may also be wise to perform diffusion imaging towards the end of the exam as the high pitched gradient sounds accompanying EPI scans can easily waken a sleeping fetus.

From a clinical standpoint, the most useful diffusion parameter is the ADC (in convenient units of $\mu m^2/ms$), which shows acute and subacute tissue injury from a variety of causes, including stroke (100). The importance of such an assessment in fetal brain MRI is obvious and several attempts have been made to perform fetal brain diffusion imaging (101–113). The inherent sensitivity to all motion, however, generally means that successful fetal diffusion brain imaging is primarily demonstrated in fetuses with pelvic head engagement

(104) or in fetuses with low fetal activity due to the use of maternal sedation (110). Even with sedation and/or fetal head engagement, residual motion artifacts due to maternal breathing and small fetal movements can significantly degrade fetal diffusion-weighted imaging. As a consequence, most fetal DWI studies have reported only crude ADC values with the more sophisticated diffusion analyses yielding directional information, such as the fractional aniosotropy (FA) and/or related tractography results being more difficult to achieve. Figure 13 shows coronal slices of a fetal DWI scan of a 39-week fetus including the computed ADC, FA, and color FA maps. The fetus was relatively quiet during this scan so diagnostic quality ADC images were obtained. Small motion artifacts significantly degraded the FA maps. This example highlights the need for motion correction in fetal DWI and indeed, some valuable recent work on the correction of inter-slice motion and fetal DWI reconstruction has been performed (110, 114, 115) which will be discussed further in Section 3.c.

We have attempted some ambitious fetal brain diffusion imaging with single-shot DWI-EPI using 12 to 32 gradient directions, b factors anywhere from 400 to 700 s/mm^2, TR values between 6 to 12 seconds, TE between 60 to 100 ms, FOV's between 250 to 300 mm^2, matrix size between 128×128 to 150×150, and slice thicknesses from 2 to 4 mm. The b values used for fetal brain are generally less than those used in the adult brain due to the generally higher diffusion coefficients found in the former (38). For 3D motion correction and analysis multiple DWI scans in the axial or coronal slice select directions have been performed with total scan times between 3 to 7 minutes. Figure 14 shows an axial SST2W image and the ADC and color FA maps of a 36-week gestation age fetus with dural sinus fistula. The images acquired for this fetus showed enlargement of the torcular and transverse sinuses with dural arteriovenous fistula/malformation, but with no evidence of brain injury. The ADC and color FA maps also confirmed intact corpus callosum and no evidence of white matter injury, which led to good neurodevelopment prognosis in this fetus. This was compatible with postnatal imaging and outcomes. For best results DWI scans should be analyzed with post-processing methods that include motion correction and reconstruction to assess white matter structure and connectivity. By using motion correction techniques it has been possible to detect and visualize corticospinal tracts, thalamocortical tracts, sensorimotor pathways, and the corpus callosum tracts using in-vivo fetal DWI (104, 107, 108, 115, 116). The spatial resolution and quality of fetal DWI and its robustness to motion remain to be improved. Data from in-vitro DWI and histology (117–122) may be used as reference to confirm in-vivo DWI and tractography findings.

Diffusion imaging of the fetal lung has also been examined as a potential tool for assessing lung maturity with somewhat mixed results. Lung measures of diffusion parameters may reflect both capillary perfusion and water diffusion in the extracellular, extravascular space and can potentially demonstrate lung maturity and functionality. Fetal lung DWI will of course also suffer from intermittent fetal motion. Maternal sedation or retrospective inter-slice motion correction may be used to reduce motion artifacts. The first report of an increase in ADC with gestation age (GA) (123) utilized DWI with low b-factors and was performed at 0.5 T in 26 fetuses, from 19 to 39 weeks GA. In another study published in 2008 (124) the "best motion-artifact-free coronal slice that displayed the large surface of the lungs" was used to measure ADC and no significant correlation was found between ADC

and GA based on DWI of 53 fetuses with normal lungs. A high b factor of 700 s/mm^2 was employed in this study. In another 2008 article (125) a highly correlated increase of ADC with GA was measured using EPI-DWI in 50 fetuses, deemed to have normal lung development, from 18 to 36 weeks GA. An impressive Pearson correlation figure from the linear regression of ADC vs. GA, r=0.816, was reported. The positive slope of ADC with GA was not explicitly provided but from the scatterplot and accompanying Table, a linear growth of ADC from around 1.6 to 3.5 μm^2/ms appears to occur over the 18 to 35 week GA range. The authors suggest that increased fluid secretion from pulmonary epithelium, "massive angiogenesis surrounding the alveoli", and an unbinding of fluid from hyaluronic acid with lung development may all contribute to an increasing ADC with GA, making ADC a potentially useful marker for lung maturity. Finally, in 2009 Cannie et al. (126) carried out a study based on six different b values (b=0, 100, 250, 500, 750, and 1000 s/mm^2) and found a positive correlation between ADC calculated at low b values with GA and a negative correlation between ADC calculated at high b values with GA. They showed that these opposite effects canceled each other when average ADC was calculated. Important information may be carried by the ADC at both low and high b values in the range of 0 to 700 s/mm^2.

e. Magnetic Resonance Spectroscopy

Magnetic resonance spectroscopy (MRS) of the proton has been used to detect changes in brain metabolites, i.e. N-acetylaspartate, choline, myo-inositol, creatine, lactate, and glutamate, during early brain development throughout gestation (127–135). Of course these metabolites of the brain are some 10,000 times less abundant than the water and fat molecules used to generate the signals from which MR images are made so that 1H MRS is generally performed very differently than MRI, albeit with the same equipment. Specifically, the simplest approach is to perform single voxel MRS methods in which three orthogonal slice selective pulses define a region, typically 1 cm^3 or larger, from which metabolic information is extracted and the water signal suppressed. The metabolic information appears as a proton spectrum in which the signals from the different metabolites appear at specific frequencies, or ppm values, within the spectrum. The two main techniques that have been used in fetal MRS are single voxel Stimulated Echo Acquisition Mode (STEAM) sequences comprised of three slice selective 90° pulses and single voxel Point Resolved Spectroscopy (PRESS) sequences consisting of a slice selective 90° pulse and two orthogonal slice selective 180° refocusing pulses. STEAM is typically used for short TE values (20 to 30 ms) and a richer metabolic content while PRESS is typically used for longer TE values, e.g. 135 ms, with less metabolic information (i.e., loss of signal from metabolites with shorter T2 relaxation time constants) but generally more interpretable and reproducible spectra. Repetition times (TR's) on the order of 1.5 to 2.5 seconds allow for sufficient T1 relaxation between signal averages and, with some 30 signal averages, lead to scan times on the order of a minute for single voxel on the order 15×15×15 mm^3 with acceptable metabolite SNR.

Metabolic changes in the brain may precede functional and structural brain abnormalities and early detection of lactate and/or glutamate levels in fetuses at risk for hypoxic-ischemic encephalopathy, achieved with MRS may thus prove quite useful. Changes in brain

metabolites and deviations from normative values may also be useful for early detection of neuronal damage. Normal changes of the metabolites have been studied during brain maturation and the myelination process; N-acetylaspartate gradually increases and choline slowly decreases during the process of myelination throughout the third trimester (131, 133). Creatine has been shown to increase with GA in 58 fetuses in the GA range of 22–39 weeks; but this was only observed at a short TE (30 msec) and was not observed at the longer TE of 135 msec.

Figure 15 and Figure 16 present brain spectra from a 20-week GA fetus and a 33-week GA fetus, respectively. Prominent resonances from creatine and NAA are seen at 33 weeks. There is perhaps an inverted doublet from lactate at 33 weeks as well. Lactate has a negative in-phase doublet at TE=144ms, and a positive in-phase doublet at TE=288ms (39), but these were not detected in earlier studies on normal fetal brain development (128, 131); however, an elevated value of lactate has shown to be present in conditions such as gastroschesis and IUGR (132, 135). The significance of the lactate peak in fetal brain pathology remains to be further studied. It is important to bear spatial interference effects (136) in mind when choosing timing parameters for lactate spectroscopy. For a comprehensive review of the human fetal brain chemistry with MRS the reader is referred to (133). MRS can also be used in evaluating other fetal organs, for example in detecting lipid peak in the fetal liver (137), and surfactant/albumin in the fetal lung (138). It may also be a useful tool in evaluating the maturity and function of the fetal heart, liver, and lung; however these applications seem to be extremely difficult due to the small size of the structures and intermittent fetal and maternal motion.

3. Other Considerations

In the current clinical environment of most care centers fetal imaging and assessment is primarily performed with ultrasound. MRI is more expensive and more difficult to schedule. Also unlike ultrasound, where pleasant discussions between examiner and examinee can take place in a private setting, MRI is performed in a constrained, claustrophobic, somewhat alien environment with documented psychological distress levels (139). On the other hand, the MR exam itself, when performed with standard safety screening protocols for exclusion, is, in our view, safe for both mother and fetus at currently available clinical field strengths up to 3 Tesla. Given the additional value of MRI as a complement to ultrasound, this risk-benefit interplay should be taken into account when choosing MRI. In this section we discuss the safety concerns, hardware updates including high magnetic fields and multi-channel coils, and motion correction and post-processing strategies.

a. Safety Concerns

Among the safety concerns related to fetal MRI are the risks of peripheral nerve stimulation, exposure to acoustic noise, and exposure to radiofrequency energy. Nonetheless, there is no evidence for any adverse effect of MRI during pregnancy on the developing fetus. There is also no special consideration for scanning during the first trimester among others, but MRI is not usually recommended during the first trimester, first because the risk of spontaneous abortion is relatively high in this period, making MRI findings moot and potentially leading to a false association between early MRI and spontaneous abortion, and second because the

spatial resolution of MRI may not be sufficient for detecting abnormalities at this early age because the fetus is so small.

The main safety concern in fetal MRI is the absorption of sufficient radiofrequency (RF) energy to harm the fetus or mother (38, 70, 73, 74). For this reason scanning is performed within standard limits for the Specific Absorption Rate (SAR) (68, 72) which is a measure of RF energy per unit time per kg (watts/kg), and is proportional to the main magnetic field strength (B_0) and the flip angle (α), as well as the RF bandwidth (Δf):

$$\mathrm{SAR} \propto \mathrm{B}_0^2 \alpha^2 \Delta f \quad (7)$$

The SST2W sequence has one of the highest RF energy exposures of MR sequences. In 2001 Levine et al. (69) performed experiments to measure possible temperature rises due to SST2W acquisitions in fetal MRI of pregnant pigs. They positioned fiber optic temperature probes in the fetal pig brain, abdomen, and amniotic fluid and did not detect any temperature rise, thus concluding that fetal MRI was safe at 1.5 T with regard to RF energy deposition. Later on using a physical model of a pregnant woman and body coil, Hand et al. (71) estimated average whole-body and local SAR values for both the fetus and mother at 1.5 and 3 T. They showed that the local SAR values could exceed the safety limits of the whole body SAR set by FDA (4 W/kg) and ICNIRP (2 W/kg). This study and another study by De Wilde et al. (70) suggested that pregnant women, especially those with thermoregulation issues should be scanned with care. In a more recent study, Hand et al. (74) refined their model by adding the effects of heat conduction and found that when the maternal whole body SAR was limited to 2 W/kg, the fetal whole body SAR was less than 1.24 W/kg and 1.14 W/kg at 1.5 and 3 T, respectively. Based on these findings, they suggested limiting continuous RF exposure to 7.5 minutes. In another study, Kikuchi et al. (73) suggested limiting RF exposure to 40 minutes at whole-body SAR value of 2 W/kg and to 10 minutes at whole-body SAR value of 4 W/kg. In addition, Hayat et al. (95) suggested limiting SAR to 2 W/kg in SSFP.

Clearly fetal MRI should always be performed with the scanner set to normal-level SAR mode conditions to ensure that SAR levels are maintained in the safe range. Under such conditions a 3 T scanner may automatically pose delays between subsequently proscribed SST2W scans to maintain normal-level SAR limits. These delays are not desired as the fetus may move to a different orientation or position and compromise the desired orientation of scans. Running SST2W MRI at 3 T with longer TR values and low flip angles will result in lower exposure and less delays between scans to avoid exceeding SAR levels. Parallel RF multi-transmit technologies provide effective ways of decreasing local SAR inhomogeneity and reducing focal SAR hotspots. As new hardware is used to advance imaging, local SAR models, better thermal models of the amniotic fluid and the inclusion of local SAR calculations are recommended (140, 141). Recent studies conducted at Wayne State University in partnership with the Perinatology Research Branch of the NICHD/NIH showed that SAR levels were within the safe limits for fetal MRI at both 1.5 and 3 T, while higher SNR was achieved by performing fetal MRI at 3T (38).

b. Hardware Considerations

Just like many other MRI protocols, fetal MRI has improved during the past decade with advances in MRI hardware and software. Here we briefly discuss fetal MRI at 3 T, the use of multi-channel body and cardiac coils, parallel imaging and fast imaging through regularized reconstruction, as well as some of the current limitations. Fetal MRI has traditionally been performed on 1.5 T magnets and is probably amongst the last protocols to begin to take advantage of the benefits of 3 T and higher magnetic fields. In addition to higher magnetic field strength, the use of multi-transmit systems, multi-channel coils and parallel imaging is undoubtedly beneficial. Uncontrollable intermittent fetal motion is the most fundamental problem and is a dominating factor that can easily obscure the advantages of new hardware and software and complicate protocol optimizations. New hardware can speed up imaging and thus reduce motion effects. Careful design and use of novel fast imaging and image processing techniques can also mitigate current limitations.

Due to increased polarization of the water molecule protons at 3 T, a theoretical twofold gain in SNR is expected compared to 1.5 T. This raises new opportunities for faster imaging, improving the spatial resolution for anatomic imaging and improving image quality of typically low SNR acquisitions like diffusion imaging with EPI. Downsides of 3 T include increased susceptibility and chemical shift artifacts, potential presence of standing wave and conductivity artifacts, higher RF energy deposition, and prolonged longitudinal relaxation times (38, 142, 143) which can result in a reduction of the SNR gain. Adjustments to TR and flip angles to maintain SAR at safe levels can further compromise the higher field SNR gain. Overall, it is estimated that the practical gain in SNR at 3 T as compared to 1.5 T is more on the order of a factor of 1.5–1.7. The gain is higher in T2-weighted imaging than T1-weighted imaging, as the transverse relaxation time is relatively immune to changes in field strength.

All in all, 3T MRI enables high SNR acquisitions even at 2-mm slice thicknesses (Figure 17a) which are difficult to achieve at 1.5T with sufficient SNR. There are obvious advantages to this when tiny structural abnormalities, lesions, and hemorrhage are of interest (144).

One issue with imaging at 3 T is artifacts related to the higher RF frequencies needed. Figure 17b shows severe standing wave/conductivity artifact that appears as a dark band across the image due to severe signal dropout. This artifact is seen specifically in 3 T abdominal MRI, especially fetal MRI of patients with polyhydramnios, patients with ascites, and obese patients (142). Two phenomena contribute to this artifact. First, RF penetration is adversely affected in abdominal MRI by the high dielectric constant of fluid and body tissue. Consequently RF wavelengths reduce from 234 cm in free space to about 30 cm in the body. This reduced wavelength is comparable to the field of view (FOV) in abdominal MRI, thus causing strong signal variation across the FOV due to standing wave interference effects. Second, the rapidly changing B_1 transmit field at 3T induces circulating electric currents in highly conductive material, such as the amniotic fluid. These currents can generate local electromagnetic fields that can oppose fluctuations in the RF field. The potential for these effects is stronger with increased amniotic fluid volume (e.g. in polyhydramnios). The standing waves and the conductivity together can dramatically attenuate the RF field and

may cause severe signal dropouts, particularly towards the center of the FOV. One solution to reduce the severity of the RF penetration and conductivity artifact at 3 T is to deploy dielectric pads on the subject. Another solution is the use of multi-transmit or "parallel transmit' systems to generate a more homogeneous effective B_1 field across the FOV (38). These systems are coming on line with new scanners.

While multi-transmit systems are being installed and increasingly used in specialized centers, multi-channel receive coils are readily available in many centers. Body coils and cardiac coils with 5 to 32 channels have been routinely used in fetal MRI, and coils with 64 and 128 channels are becoming available for 3 T scanners. This approach has improved fetal imaging by shortening imaging time and reducing artifacts using parallel imaging.

Coil positioning is extremely important especially in MRS and DWI studies of the fetal brain where acquisition of high homogenous signal is crucial. Heerschap et al. (145) studied the effect of positioning the receive coil near the fetal head on fetal brain MRS and compared several coil systems including phased array body coil, Helmholtz coil, and linear and circular polarized surface coils. They concluded that a flexible linear coil was the best. In our experience a combination of phased array body coils and spinal coils or cardiac coils with 5 to 32 channels provide suitable configurations, but special attention must be paid to coil positioning to achieve high SNR in all regions of interest.

c. Motion Correction and Post-Processing

Intermittent fetal motion affects fetal MRI in several ways. First, fetal motion inhibits any prolonged k-space data acquisition, such as those usually needed in 3D MRI sequences, thus virtually limits fetal MRI to fast 2D slice acquisitions. Second, even with fast 2D scans like SST2W MRI, which are aimed at freezing the motion of the fetus at about few hundred milliseconds instant of k-space sampling for each slice acquisition, continuous and intermittent fetal motion spreads across the amniotic fluid and causes severe signal intensity and spin history artifacts that occasionally degrade the quality of slices (146). Finally, inter-slice motion results in discrepancy between slice positions, which in turn challenges any 3D post-processing that relies upon accurate volumetric spatial correspondences between voxels. Examples of such postprocessing tasks include 3D or 2D+time analysis of the anatomy as well as 3D+time or 3D+direction functional or structural connectivity analysis using functional MRI or diffusion weighted MRI, which all require establishment of exact voxel-by-voxel correspondences between scans acquired over a relatively longer period of time; these scans, based on EPI, last several hundred seconds to acquire hence are more susceptible to fetal motion. Pharmacologic intervention is performed in some centers, for example in France, to reduce fetal motion. Benzodiazepines, such as Ambien and Diazepam, are used for this purpose, however, this is undesired in clinic and is not permissible in research. Even after such interventions, residual maternal and fetal motion may severely affect the quality of fetal MRI scans. The correction of motion is thus crucial in advanced analysis and interpretation of fetal MRI data.

Prospective motion correction has been used in fetal and abdominal MRI through navigator echoes (147, 148), but the non-rigid nature, and the extent and complexity of fetal motion has made this approach challenging. In practice, the use of image-based navigators or

motion correction techniques has been more successful. The most compelling fetal motion correction techniques so far have been retrospective approaches that have integrated retrospective slice motion correction with volumetric image reconstruction (149–153). These image volume reconstruction techniques have been shown to enable high-resolution volumetric imaging of the fetal brain despite intermittent fetal and maternal motion. Pioneers of these techniques, Rousseau et al. (149) and Jiang et al. (150), combined iterations of slice-to-volume registration and scattered data interpolation for volumetric reconstruction of fetal brain MRI from multiple sets of thick-slice SST2W scans. In a more systematic approach Gholipour et al. (151) introduced a physical forward model of slice acquisition incorporating motion, slice profile, and sampling, and then solved an inverse problem to reconstruct a high-resolution volume from multiple slice acquisitions. More recently, Kuklisova-Murgasova et al. (153) developed an expectation maximization formulation of this approach and incorporated inter-slice intensity matching and complete outlier removal in volume reconstruction. High-quality, high-resolution volumetric images of the fetal brain were achieved by this approach from multiple SST2W scans obtained with 2-mm slice thickness.

The correction of motion in DWI and functional MRI studies is more challenging, first because of a fourth dimension (time to acquire fMRI data or direction of diffusion sensitizing gradients for DWI) added to the study, and second because of the inherent susceptibility of EPI to magnetic field inhomogeneity which causes geometric distortion, and motion-induced spin history artifacts. In this direction there has been invaluable body of work on DWI motion correction and reconstruction (110, 114, 115). The essence of these methods is also slice-by-slice motion correction and scattered data interpolation (SDI) in image space and q-space. The first technique, developed by Jiang et al. (114), was built upon a 6-parameter rank-2 tensor model, by which they found differences in ADC and FA between fetuses with normal brain and fetuses with brain anomalies such as agenesis of corpus callosum. Oubel et al. (110) then proposed a method to relax the dependency on a simple diffusion tensor model. In this approach spatial points and diffusion gradients were interpolated into desired target image space and q-space using separable Gaussian kernels. Both techniques rely on reconstruction from repeated fetal DWI scans acquired in one slice select direction. In a more systematic approach Fogtmann et al. developed unified registration and reconstruction from multiple DWI scans through modeling the spatial resolution of DWI slices, achieving high-resolution FA maps and tractography (115). In the functional MRI domain in the fetus, without sedation and with a total fMRI acquisition time of 1–3 minutes, Schopf et al. reported 75% subject dropout rate due to motion (154). This highlights the necessity of correcting for motion and motion-induced artifacts, such as spin history and intensity inhomogeneity artifacts, in complex analysis tasks like fetal functional MRI (155, 156).

Motion correction in fetal MRI has enabled significant new advances in volumetric and morphometric analysis of early brain development and cortical maturation (157–167). Spatiotemporal atlases of human fetal brain growth have been developed based on volumetric fetal brain MRI (41–43) and research on automatic segmentation of the fetal brain tissue and quantitative analysis has emerged (161, 164–168). Insight from histology and in-vitro MRI (117–122) provides an excellent source of information and reference for

the evaluation of in-vivo MRI findings. The main advantage of *in-vitro* MRI is its excellent spatial resolution (about 100 μm), which is feasible due to the absence of subject motion and unlimited acquisition time. In-vivo fetal MRI, however, as a non-invasive diagnostic imaging technique, has great potential to not only advance our knowledge but also to improve the management of high-risk pregnancies and the diagnosis and treatment of congenital anomalies. Improving the spatial resolution and contrast of fetal MRI, decreasing its sensitivity to motion, and reducing the total acquisition time and energy deposition remain top priorities in technology development.

4. Conclusion

Fetal MRI is challenging due to the small size of fetal organs and by intermittent fetal and maternal motion that disrupt the spatial encoding needed for 3D image acquisition. Scanning approaches thus most usually employ fast 2D imaging sequences to freeze the motion with the single shot fast spin echo T2-weighted (SST2W) sequence constituting the primary method for clinical evaluation of congenital anomalies. This sequence provides a highly T2-weighted contrast which is excellent for the evaluation of most fetal organs, including the fetal brain, lung, abdomen, urinary tract, as well as musculoskeletal and craniofacial structures. Other sequences that may also employed include inversion recovery T1-weighted MRI to detect hemorrhage, unspoiled gradient echo SSFP for structural surveys and cinematographic imaging. Diffusion-weighted MRI and functional MRI may be useful for evaluation of function-structure relationships, and MRS in the analysis of metabolites. For all sequences, it is crucial to fine tune sequence parameters in fetal MRI. This includes the TR, TE, flip angle, matrix size, and slice thickness.

Table 1 shows typical parameters of our fetal MRI protocol as implemented on a 3T scanner. These parameters may be changed based on scan conditions, clinical indication, and the fetal and maternal size. The sequences have been sorted in their perceived relative importance and are typically applied in this order; however, this may change depending on the clinical indication. It is difficult to overemphasize the value of employing interactive fetal MRI scan sessions in which the position of the fetus is updated by the last slice of a scan, with the next scan beginning immediately after by eliminating auto-prescan to minimize the time between scans with similar sequences. This approach maximizes the chance of acquiring high quality images with a minimum of non-usable data. We noted that SST2W sequence is the front-line fetal imaging technique from which the majority of the information about anatomy is achieved. It is noteworthy that SSFP may be used as an alternative to SST2W imaging for structural survey when severe artifacts such as standing waves and conductivity artifacts or excessive RF energy deposition become barriers, particularly at 3 T. SSFP is, however, more sensitive to motion, exhibits limited tissue contrast, and often can have banding artifacts.

Fetal MRI is safe at 1.5 T and 3 T if performed under normal-level SAR mode. Imaging at 3 T offers a gain of about 1.5–1.7 fold in SNR, but at the expense of potential artifacts related to standing waves and conductivity which cause signal dropout appearing as dark bands in images. This artifact is particularly seen in patients with excess amniotic fluid and may be reduced by multi-transmit systems or by using dielectric pads.

New hardware, in specific multi-transmit systems and multi-channel receive coils, are anticipated to significantly accelerate and improve fetal MRI. In addition, motion correction has become increasingly useful in merging fetal MRI scans for post-processing, with an invaluable body of work developed on motion correction and volumetric reconstruction from fast 2D slice acquisitions. This has enabled significant advances in the analysis of early brain development, cortical maturation, and connectivity. Nevertheless, in-vivo analysis of fetal brain growth and detection of subtle abnormalities remain active and challenging areas of research. Intermittent fetal motion and limited spatial resolution still present major challenges for assessing fetal anatomy in-utero using in-vivo fetal MRI.

Acknowledgments

This work was in part supported by National Institutes of Health (NIH) grants R01EB018988, R01EB013248, R01LM010033, R03DE22109, and the Harvard Catalyst-Harvard Clinical and Translational Science Center for Research Resources and the National Center for Advancing Translational Sciences, award UL1TR001102.

References

1. Levine D, Barnes PD, Madsen JR, Li W, Edelman RR. Fetal central nervous system anomalies: MR imaging augments sonographic diagnosis. Radiology. 1997; 204(3):635–42. [PubMed: 9280237]
2. Levine D, Barnes PD, Sher S, Semelka RC, Li W, McArdle CR, Worawattanakul S, Edelman RR. Fetal fast MR imaging: reproducibility, technical quality, and conspicuity of anatomy. Radiology. 1998; 206(2):549–54. [PubMed: 9457211]
3. Levine D, Barnes PD, Edelman RR. Obstetric MR imaging. Radiology. 1999; 211(3):609–17. [PubMed: 10352581]
4. Huppert BJ, Brandt KR, Ramin KD, King BF. Single-shot fast spin-echo MR imaging of the fetus: a pictorial essay. Radiographics. 1999; 19(Spec No):S215–27. [PubMed: 10517456]
5. Coakley FV, Glenn OA, Qayyum A, Barkovich AJ, Goldstein R, Filly RA. Fetal MRI: a developing technique for the developing patient. AJR Am J Roentgenol. 2004; 182(1):243–52. [PubMed: 14684546]
6. Levine D. Obstetric MRI. J Magn Reson Imaging. 2006; 24(1):1–15. [PubMed: 16736491]
7. Pugash D, Brugger PC, Bettelheim D, Prayer D. Prenatal ultrasound and fetal MRI: the comparative value of each modality in prenatal diagnosis. Eur J Radiol. 2008; 68(2):214–26. [PubMed: 18790583]
8. Reddy UM, Filly RA, Copel JA. Prenatal imaging: ultrasonography and magnetic resonance imaging. Obstet Gynecol. 2008; 112(1):145–57. [PubMed: 18591320]
9. Avni FE, Massez A, Cassart M. Tumours of the fetal body: a review. Pediatr Radiol. 2009; 39(11): 1147–57. [PubMed: 19238373]
10. Levine D, Barnes PD, Madsen JR, Abbott J, Mehta T, Edelman RR. Central nervous system abnormalities assessed with prenatal magnetic resonance imaging. Obstet Gynecol. 1999; 94(6): 1011–9. [PubMed: 10576192]
11. Lan LM, Yamashita Y, Tang Y, Sugahara T, Takahashi M, Ohba T, Okamura H. Normal fetal brain development: MR imaging with a half-Fourier rapid acquisition with relaxation enhancement sequence. Radiology. 2000; 215(1):205–10. [PubMed: 10751488]
12. Huisman TA, Martin E, Kubik-Huch R, Marincek B. Fetal magnetic resonance imaging of the brain: technical considerations and normal brain development. Eur Radiol. 2002; 12(8):1941–51. [PubMed: 12136312]
13. Levine D, Barnes PD, Robertson RR, Wong G, Mehta TS. Fast MR imaging of fetal central nervous system abnormalities. Radiology. 2003; 229(1):51–61. [PubMed: 12920177]
14. Glenn OA, Barkovich AJ. Magnetic resonance imaging of the fetal brain and spine: an increasingly important tool in prenatal diagnosis, part 1. AJNR Am J Neuroradiol. 2006; 27(8):1604–11. [PubMed: 16971596]

15. Glenn OA, Barkovich J. Magnetic resonance imaging of the fetal brain and spine: an increasingly important tool in prenatal diagnosis: part 2. AJNR Am J Neuroradiol. 2006; 27 (9):1807–14. [PubMed: 17032846]
16. Garel C. New advances in fetal MR neuroimaging. Pediatr Radiol. 2006; 36(7):621–5. [PubMed: 16770666]
17. Limperopoulos C, Robertson RL Jr, Khwaja OS, Robson CD, Estroff JA, Barnewolt C, Levine D, Morash D, Nemes L, Zaccagnini L, du Plessis AJ. How accurately does current fetal imaging identify posterior fossa anomalies? AJR Am J Roentgenol. 2008; 190(6):1637–43. [PubMed: 18492918]
18. Guibaud L. Contribution of fetal cerebral MRI for diagnosis of structural anomalies. Prenat Diagn. 2009; 29(4):420–33. [PubMed: 19156685]
19. Rutherford MA. Magnetic resonance imaging of the fetal brain. Curr Opin Obstet Gynecol. 2009; 21(2):180–6. [PubMed: 19996870]
20. Glenn OA. MR imaging of the fetal brain. Pediatr Radiol. 2010; 40(1):68–81. [PubMed: 19937234]
21. Brugger PC, Prayer D. Fetal abdominal magnetic resonance imaging. Eur J Radiol. 2006; 57(2): 278–93. [PubMed: 16388926]
22. Kasprian G, Balassy C, Brugger PC, Prayer D. MRI of normal and pathological fetal lung development. Eur J Radiol. 2006; 57(2):261–70. [PubMed: 16413987]
23. Nemec SF, Nemec U, Brugger PC, Bettelheim D, Rotmensch S, Graham JM Jr, Rimoin DL, Prayer D. MR imaging of the fetal musculoskeletal system. Prenat Diagn. 2012; 32(3):205–13. [PubMed: 22430716]
24. Abramowicz JS, Sheiner E. In utero imaging of the placenta: importance for diseases of pregnancy. Placenta. 2007; 28 (Suppl A):S14–22. [PubMed: 17383721]
25. Damodaram M, Story L, Eixarch E, Patel A, McGuinness A, Allsop J, Wyatt-Ashmead J, Kumar S, Rutherford M. Placental MRI in intrauterine fetal growth restriction. Placenta. 2010; 31(6):491–8. [PubMed: 20347139]
26. Lim PS, Greenberg M, Edelson MI, Bell KA, Edmonds PR, Mackey AM. Utility of ultrasound and MRI in prenatal diagnosis of placenta accreta: a pilot study. AJR Am J Roentgenol. 2011; 197(6): 1506–13. [PubMed: 22109309]
27. Derman AY, Nikac V, Haberman S, Zelenko N, Opsha O, Flyer M. MRI of placenta accreta: a new imaging perspective. AJR Am J Roentgenol. 2011; 197(6):1514–21. [PubMed: 22109310]
28. Maher MA, Abdelaziz A, Bazeed MF. Diagnostic accuracy of ultrasound and MRI in the prenatal diagnosis of placenta accreta. Acta Obstet Gynecol Scand. 2013; 92(9):1017–22. [PubMed: 23711014]
29. El Jack AK, Siegelman ES. “Pseudoseptum” of the uterine cervix on MRI. J Magn Reson Imaging. 2007; 26(4):963–5. [PubMed: 17896350]
30. Sala E, Wakely S, Senior E, Lomas D. MRI of malignant neoplasms of the uterine corpus and cervix. AJR Am J Roentgenol. 2007; 188(6):1577–87. [PubMed: 17515380]
31. Donaldson SB, West CM, Davidson SE, Carrington BM, Hutchison G, Jones AP, Sourbron SP, Buckley DL. A comparison of tracer kinetic models for T1-weighted dynamic contrast-enhanced MRI: application in carcinoma of the cervix. Magn Reson Med. 2010; 63(3):691–700. [PubMed: 20187179]
32. Stenstedt K, Hellstrom AC, Fridsten S, Blomqvist L. Impact of MRI in the management and staging of cancer of the uterine cervix. Acta Oncol. 2011; 50(3):420–6. [PubMed: 21166605]
33. Prayer D, Brugger PC, Prayer L. Fetal MRI: techniques and protocols. Pediatr Radiol. 2004; 34(9): 685–93. [PubMed: 15316689]
34. Huisman TA. Fetal magnetic resonance imaging. Semin Roentgenol. 2008; 43(4):314–36. [PubMed: 18774035]
35. Limperopoulos, C.; Clouchoux, C. Seminars in perinatology. Elsevier; 2009. Advancing fetal brain MRI: targets for the future.
36. Prayer D, Fetal MRI. Top Magn Reson Imaging. 2011; 22(3):89. [PubMed: 23558462]

37. Laifer-Narin S, Budorick NE, Simpson LL, Platt LD. Fetal magnetic resonance imaging: a review. Curr Opin Obstet Gynecol. 2007; 19(2):151–6. [PubMed: 17353684]
38. Welsh RC, Nemec U, Thomason ME. Fetal Magnetic Resonance Imaging at 3. 0 T. Topics in Magnetic Resonance Imaging. 2011; 22(3):119–131. [PubMed: 23558467]
39. Soman S, Kasprian G, Schopf V, Berger-Kulemann V, Nemec U, Mitter C, Prayer D. Advanced fetal MRI: Diffusion tensor imaging, spectroscopy, dynamic MRI, resting-state functional MRI. Journal of Pediatric Neuroradiology. 2012; 1(3):225–251.
40. Chapman T, Matesan M, Weinberger E, Bulas DI. Digital atlas of fetal brain MRI. Pediatr Radiol. 2010; 40(2):153–62. [PubMed: 19774370]
41. Habas PA, Kim K, Corbett-Detig JM, Rousseau F, Glenn OA, Barkovich AJ, Studholme C. A spatiotemporal atlas of MR intensity, tissue probability and shape of the fetal brain with application to segmentation. Neuroimage. 2010; 53(2):460–70. [PubMed: 20600970]
42. Serag A, Aljabar P, Ball G, Counsell SJ, Boardman JP, Rutherford MA, Edwards AD, Hajnal JV, Rueckert D. Construction of a consistent high-definition spatio-temporal atlas of the developing brain using adaptive kernel regression. Neuroimage. 2012; 59(3):2255–65. [PubMed: 21985910]
43. Gholipour A, Limperopoulos C, Clancy S, Clouchoux C, Akhondi-Asl A, Estroff JA, Warfield SK. Construction of a deformable spatiotemporal MRI atlas of the fetal brain: evaluation of similarity metrics and deformation models. Med Image Comput Comput Assist Interv. 2014; 17(Pt 2):292–9. [PubMed: 25485391]
44. Grossman R, Hoffman C, Mardor Y, Biegon A. Quantitative MRI measurements of human fetal brain development in utero. Neuroimage. 2006; 33(2):463–70. [PubMed: 16938471]
45. Parazzini C, Righini A, Rustico M, Consonni D, Triulzi F. Prenatal magnetic resonance imaging: brain normal linear biometric values below 24 gestational weeks. Neuroradiology. 2008; 50(10): 877–83. [PubMed: 18563404]
46. Hatab MR, Zaretsky MV, Alexander JM, Twickler DM. Comparison of fetal biometric values with sonographic and 3D reconstruction MRI in term gestations. AJR Am J Roentgenol. 2008; 191(2): 340–5. [PubMed: 18647899]
47. Tilea B, Alberti C, Adamsbaum C, Armoogum P, Oury JF, Cabrol D, Sebag G, Kalifa G, Garel C. Cerebral biometry in fetal magnetic resonance imaging: new reference data. Ultrasound Obstet Gynecol. 2009; 33(2):173–81. [PubMed: 19172662]
48. Vossough A, Limperopoulos C, Putt ME, du Plessis AJ, Schwab PJ, Wu J, Gee JC, Licht DJ. Development and validation of a semiquantitative brain maturation score on fetal MR images: initial results. Radiology. 2013; 268(1):200–7. [PubMed: 23440324]
49. Santiago Medina L, Mulkern RV, Strife KR, Zurakowski D, Barnes PD. Database prescan: a time-efficient alternative to brain MRI autoprescan. J Magn Reson Imaging. 1997; 7(2):442–6. [PubMed: 9090606]
50. Daffos F, Forestier F, Mac Aleese J, Aufrant C, Mandelbrot L, Cabanis EA, Iba-Zizen MT, Alfonso JM, Tamraz J. Fetal curarization for prenatal magnetic resonance imaging. Prenat Diagn. 1988; 8(4):312–4. [PubMed: 2969509]
51. Revel MP, Pons JC, Lelaidier C, Fournet P, Vial M, Musset D, Labrune M, Frydman R. Magnetic resonance imaging of the fetus: a study of 20 cases performed without curarization. Prenat Diagn. 1993; 13(9):775–99. [PubMed: 8278309]
52. Girard N, Raybaud C, Dercole C, Boubli L, Chau C, Cahen S, Potier A, Gamerre M. In vivo MRI of the fetal brain. Neuroradiology. 1993; 35(6):431–436. [PubMed: 8377914]
53. Shakespeare W. Invasive Fetal Procedures. Operative obstetrics. 1995:76.
54. Mansfield P, Stehling MK, Ordidge RJ, Coxon R, Chapman B, Blamire A, Gibbs P, Johnson IR, Symonds EM, Worthington BS, et al. Echo planar imaging of the human fetus in utero at 0. 5 T. Br J Radiol. 1990; 63(755):833–41. [PubMed: 2252974]
55. Stehling MK, Mansfield P, Ordidge RJ, Coxon R, Chapman B, Blamire A, Gibbs P, Johnson IR, Symonds EM, Worthington BS, et al. Echo-planar imaging of the human fetus in utero. Magn Reson Med. 1990; 13(2):314–8. [PubMed: 2314220]
56. Baker PN, Johnson IR, Gowland PA, Hykin J, Adams V, Mansfield P, Worthington BS. Measurement of fetal liver, brain and placental volumes with echo-planar magnetic resonance imaging. Br J Obstet Gynaecol. 1995; 102(1):35–9. [PubMed: 7833308]

57. Duncan KR, Gowland PA, Moore RJ, Baker PN, Johnson IR. Assessment of fetal lung growth in utero with echo-planar MR imaging. Radiology. 1999; 210(1):197–200. [PubMed: 9885608]
58. Mesrur Halefoglu, A. Seminars in roentgenology. WB Saunders; 2008. Magnetic resonance cholangiopancreatography.
59. Mulkern RV, Wong ST, Winalski C, Jolesz FA. Contrast manipulation and artifact assessment of 2D and 3D RARE sequences. Magn Reson Imaging. 1990; 8(5):557–66. [PubMed: 2082125]
60. Mulkern RV, Melki PS, Jakab P, Higuchi N, Jolesz FA. Phase-encode order and its effect on contrast and artifact in single-shot RARE sequences. Med Phys. 1991; 18(5):1032–7. [PubMed: 1961143]
61. Chien D, Mulkern RV. Fast spin-echo studies of contrast and small-lesion definition in a liver-metastasis phantom. J Magn Reson Imaging. 1992; 2(4):483–7. [PubMed: 1633403]
62. Melki PS, Jolesz FA, Mulkern RV. Partial RF echo-planar imaging with the FAISE method. II. Contrast equivalence with spin-echo sequences. Magn Reson Med. 1992; 26 (2):342–54. [PubMed: 1513255]
63. Melki PS, Jolesz FA, Mulkern RV. Partial RF echo planar imaging with the FAISE method. I. Experimental and theoretical assessment of artifact. Magn Reson Med. 1992; 26 (2):328–41. [PubMed: 1513254]
64. Constable RT, Anderson AW, Zhong J, Gore JC. Factors influencing contrast in fast spin-echo MR imaging. Magn Reson Imaging. 1992; 10(4):497–511. [PubMed: 1501520]
65. Leppert IR, Almli CR, McKinstry RC, Mulkern RV, Pierpaoli C, Rivkin MJ, Pike GB. T(2) relaxometry of normal pediatric brain development. J Magn Reson Imaging. 2009; 29 (2):258–67. [PubMed: 19161173]
66. Mulkern, RV. MR Imaging of the Brain and Spine. 3. Philadelphia: Lippincott Williams & Wilkins; 2002. Fast imaging principles; p. 176-78.
67. Melki PS, Mulkern RV. Magnetization transfer effects in multislice RARE sequences. Magn Reson Med. 1992; 24(1):189–95. [PubMed: 1556927]
68. Gandhi OP, Chen XB. Specific absorption rates and induced current densities for an anatomy-based model of the human for exposure to time-varying magnetic fields of MRI. Magn Reson Med. 1999; 41(4):816–23. [PubMed: 10332859]
69. Levine D, Zuo C, Faro CB, Chen Q. Potential heating effect in the gravid uterus during MR HASTE imaging. J Magn Reson Imaging. 2001; 13(6):856–61. [PubMed: 11382944]
70. De Wilde JP, Rivers AW, Price DL. A review of the current use of magnetic resonance imaging in pregnancy and safety implications for the fetus. Prog Biophys Mol Biol. 2005; 87(2–3):335–53. [PubMed: 15556670]
71. Hand JW, Li Y, Thomas EL, Rutherford MA, Hajnal JV. Prediction of specific absorption rate in mother and fetus associated with MRI examinations during pregnancy. Magn Reson Med. 2006; 55(4):883–93. [PubMed: 16508913]
72. Wang Z, Lin JC, Mao W, Liu W, Smith MB, Collins CM. SAR and temperature: simulations and comparison to regulatory limits for MRI. J Magn Reson Imaging. 2007; 26 (2):437–41. [PubMed: 17654736]
73. Kikuchi S, Saito K, Takahashi M, Ito K. Temperature elevation in the fetus from electromagnetic exposure during magnetic resonance imaging. Phys Med Biol. 2010; 55(8):2411–26. [PubMed: 20360633]
74. Hand JW, Li Y, Hajnal JV. Numerical study of RF exposure and the resulting temperature rise in the foetus during a magnetic resonance procedure. Phys Med Biol. 2010; 55(4):913–30. [PubMed: 20090188]
75. Mugler JP 3rd, Bao S, Mulkern RV, Guttmann CR, Robertson RL, Jolesz FA, Brookeman JR. Optimized single-slab three-dimensional spin-echo MR imaging of the brain. Radiology. 2000; 216(3):891–9. [PubMed: 10966728]
76. Hennig J, Weigel M, Scheffler K. Multiecho sequences with variable refocusing flip angles: optimization of signal behavior using smooth transitions between pseudo steady states (TRAPS). Magn Reson Med. 2003; 49(3):527–35. [PubMed: 12594756]

77. Hennig J, Weigel M, Scheffler K. Calculation of flip angles for echo trains with predefined amplitudes with the extended phase graph (EPG)-algorithm: principles and applications to hyperecho and TRAPS sequences. Magn Reson Med. 2004; 51(1):68–80. [PubMed: 14705047]
78. Busse RF. Reduced RF power without blurring: correcting for modulation of refocusing flip angle in FSE sequences. Magn Reson Med. 2004; 51(5):1031–7. [PubMed: 15122687]
79. Busse RF, Hariharan H, Vu A, Brittain JH. Fast spin echo sequences with very long echo trains: design of variable refocusing flip angle schedules and generation of clinical T2 contrast. Magnetic resonance in medicine. 2006; 55(5):1030–1037. [PubMed: 16598719]
80. Schoenberg, SO.; Dietrich, O.; Reiser, MF. Parallel imaging in clinical MR applications. Springer; 2007.
81. Yuan J, Zhao TC, Tang Y, Panych LP. Reduced field-of-view single-shot fast spin echo imaging using two-dimensional spatially selective radiofrequency pulses. J Magn Reson Imaging. 2010; 32(1):242–8. [PubMed: 20578031]
82. Finsterbusch J. Fast-spin-echo imaging of inner fields-of-view with 2D-selective RF excitations. Journal of Magnetic Resonance Imaging. 2010; 31(6):1530–1537. [PubMed: 20512911]
83. Malamateniou C, McGuinness AK, Allsop JM, O'Regan DP, Rutherford MA, Hajnal JV. Snapshot inversion recovery: an optimized single-shot T1-weighted inversion-recovery sequence for improved fetal brain anatomic delineation. Radiology. 2011; 258(1):229–35. [PubMed: 20980451]
84. Constable RT, Gore JC. The loss of small objects in variable TE imaging: implications for FSE, RARE, and EPI. Magnetic resonance in medicine. 1992; 28(1):9–24. [PubMed: 1435225]
85. Scheffler K, Lehnhardt S. Principles and applications of balanced SSFP techniques. European radiology. 2003; 13(11):2409–2418. [PubMed: 12928954]
86. Scheffler K, Hennig J. Is TrueFISP a gradient-echo or a spin-echo sequence? Magn Reson Med. 2003; 49(2):395–7. [PubMed: 12541263]
87. Zur Y, Wood M, Neuringer L. Spoiling of transverse magnetization in steady-state sequences. Magnetic resonance in medicine. 1991; 21(2):251–263. [PubMed: 1745124]
88. Ma J, Wehrli FW. Method for image-based measurement of the reversible and irreversible contribution to the transverse-relaxation rate. Journal of Magnetic Resonance, Series B. 1996; 111(1):61–69. [PubMed: 8620286]
89. Mulkern RV, Balasubramanian M, Orbach DB, Mitsouras D, Haker SJ. Incorporating reversible and irreversible transverse relaxation effects into Steady State Free Precession (SSFP) signal intensity expressions for fMRI considerations. Magn Reson Imaging. 2013; 31(3):346–52. [PubMed: 23337079]
90. Rivkin MJ, Wolraich D, Als H, McAnulty G, Butler S, Conneman N, Fischer C, Vajapeyam S, Robertson RL, Mulkern RV. Prolonged T*2 values in newborn versus adult brain: Implications for fMRI studies of newborns. Magn Reson Med. 2004; 51(6):1287–91. [PubMed: 15170852]
91. Rofsky NM, Lee VS, Laub G, Pollack MA, Krinsky GA, Thomasson D, Ambrosino MM, Weinreb JC. Abdominal MR imaging with a volumetric interpolated breath-hold examination. Radiology. 1999; 212(3):876–84. [PubMed: 10478260]
92. Bader TR, Semelka RC, Pedro MS, Armao DM, Brown MA, Molina PL. Magnetic resonance imaging of pulmonary parenchymal disease using a modified breath-hold 3D gradient-echo technique: initial observations. J Magn Reson Imaging. 2002; 15(1):31–8. [PubMed: 11793454]
93. Inaoka T, Sugimori H, Sasaki Y, Takahashi K, Sengoku K, Takada N, Aburano T. VIBE MRI for evaluating the normal and abnormal gastrointestinal tract in fetuses. AJR Am J Roentgenol. 2007; 189(6):W303–8. [PubMed: 18029839]
94. Mulkern RV, Chung T. From signal to image: magnetic resonance imaging physics for cardiac magnetic resonance. Pediatr Cardiol. 2000; 21(1):5–17. [PubMed: 10672610]
95. Hayat TT, Nihat A, Martinez-Biarge M, McGuinness A, Allsop JM, Hajnal JV, Rutherford MA. Optimization and initial experience of a multisection balanced steady-state free precession cine sequence for the assessment of fetal behavior in utero. AJNR Am J Neuroradiol. 2011; 32(2):331–8. [PubMed: 21087938]
96. Shen SH, Guo WY, Hung JH. Two-dimensional fast imaging employing steady-state acquisition (FIESTA) cine acquisition of fetal non-central nervous system abnormalities. J Magn Reson Imaging. 2007; 26(3):672–7. [PubMed: 17729346]

97. Guo WY, Ono S, Oi S, Shen SH, Wong TT, Chung HW, Hung JH. Dynamic motion analysis of fetuses with central nervous system disorders by cine magnetic resonance imaging using fast imaging employing steady-state acquisition and parallel imaging: a preliminary result. J Neurosurg. 2006; 105(2 Suppl):94–100. [PubMed: 16922069]

98. Hinshaw WS. Image formation by nuclear magnetic resonance: The sensitive-point method. Journal of Applied Physics. 1976; 47(8):3709–3721.

99. Stejskal E, Tanner J. Spin diffusion measurements: spin echoes in the presence of a time-dependent field gradient. The journal of chemical physics. 1965; 42(1):288.

100. Neumann-Haefelin T, Wittsack H-J, Wenserski F, Siebler M, Seitz RJ, Mödder U, Freund H-J. Diffusion-and perfusion-weighted MRI The DWI/PWI mismatch region in acute stroke. Stroke. 1999; 30(8):1591–1597. [PubMed: 10436106]

101. Baldoli C, Righini A, Parazzini C, Scotti G, Triulzi F. Demonstration of acute ischemic lesions in the fetal brain by diffusion magnetic resonance imaging. Ann Neurol. 2002; 52(2):243–6. [PubMed: 12210800]

102. Righini A, Bianchini E, Parazzini C, Gementi P, Ramenghi L, Baldoli C, Nicolini U, Mosca F, Triulzi F. Apparent diffusion coefficient determination in normal fetal brain: a prenatal MR imaging study. AJNR Am J Neuroradiol. 2003; 24(5):799–804. [PubMed: 12748074]

103. Bui T, Daire JL, Chalard F, Zaccaria I, Alberti C, Elmaleh M, Garel C, Luton D, Blanc N, Sebag G. Microstructural development of human brain assessed in utero by diffusion tensor imaging. Pediatr Radiol. 2006; 36(11):1133–40. [PubMed: 16960686]

104. Kasprian G, Brugger PC, Weber M, Krssak M, Krampl E, Herold C, Prayer D. In utero tractography of fetal white matter development. Neuroimage. 2008; 43(2):213–24. [PubMed: 18694838]

105. Kim DH, Chung S, Vigneron DB, Barkovich AJ, Glenn OA. Diffusion-weighted imaging of the fetal brain in vivo. Magn Reson Med. 2008; 59(1):216–20. [PubMed: 18050314]

106. Schneider MM, Berman JI, Baumer FM, Glass HC, Jeng S, Jeremy RJ, Esch M, Biran V, Barkovich AJ, Studholme C, Xu D, Glenn OA. Normative apparent diffusion coefficient values in the developing fetal brain. AJNR Am J Neuroradiol. 2009; 30(9):1799–803. [PubMed: 19556350]

107. Kasprian G, Del Rio M, Prayer D. Fetal diffusion imaging: pearls and solutions. Top Magn Reson Imaging. 2010; 21(6):387–94. [PubMed: 22158132]

108. Mitter C, Kasprian G, Brugger PC, Prayer D. Three-dimensional visualization of fetal white-matter pathways in utero. Ultrasound Obstet Gynecol. 2011; 37(2):252–3. [PubMed: 21264986]

109. Berman JI, Hamrick SE, McQuillen PS, Studholme C, Xu D, Henry RG, Hornberger LK, Glenn OA. Diffusion-weighted imaging in fetuses with severe congenital heart defects. AJNR Am J Neuroradiol. 2011; 32(2):E21–2. [PubMed: 20075085]

110. Oubel E, Koob M, Studholme C, Dietemann JL, Rousseau F. Reconstruction of scattered data in fetal diffusion MRI. Med Image Anal. 2012; 16(1):28–37. [PubMed: 21636311]

111. Hoffmann C, Weisz B, Lipitz S, Yaniv G, Katorza E, Bergman D, Biegon A. Regional apparent diffusion coefficient values in 3rd trimester fetal brain. Neuroradiology. 2014; 56(7):561–7. [PubMed: 24748534]

112. Weisz B, Hoffmann C, Ben-Baruch S, Yinon Y, Gindes L, Katorza E, Shrim A, Bar Yosef O, Schiff E, Lipitz S. Early detection by diffusion-weighted sequence magnetic resonance imaging of severe brain lesions after fetoscopic laser coagulation for twin-twin transfusion syndrome. Ultrasound Obstet Gynecol. 2014; 44(1):44–9. [PubMed: 24375775]

113. Yaniv G, Hoffmann C, Weisz B, Lipitz S, Katorza E, Kidron D, Bergman D, Biegon A. Region selective reductions in brain apparent diffusion coefficient in CMV-infected fetuses. Ultrasound Obstet Gynecol. 2014

114. Jiang S, Xue H, Counsell S, Anjari M, Allsop J, Rutherford M, Rueckert D, Hajnal JV. Diffusion tensor imaging (DTI) of the brain in moving subjects: application to in-utero fetal and ex-utero studies. Magn Reson Med. 2009; 62(3):645–55. [PubMed: 19526505]

115. Fogtmann M, Seshamani S, Kroenke C, Xi C, Chapman T, Wilm J, Rousseau F, Studholme C. A unified approach to diffusion direction sensitive slice registration and 3-D DTI reconstruction

from moving fetal brain anatomy. IEEE Trans Med Imaging. 2014; 33(2):272–89. [PubMed: 24108711]

116. Pontabry J, Rousseau F, Oubel E, Studholme C, Koob M, Dietemann JL. Probabilistic tractography using Q-ball imaging and particle filtering: application to adult and in-utero fetal brain studies. Med Image Anal. 2013; 17(3):297–310. [PubMed: 23265801]
117. Kostovic I, Judas M, Rados M, Hrabac P. Laminar organization of the human fetal cerebrum revealed by histochemical markers and magnetic resonance imaging. Cereb Cortex. 2002; 12(5): 536–44. [PubMed: 11950771]
118. Kostovic I, Vasung L. Insights from in vitro fetal magnetic resonance imaging of cerebral development. Semin Perinatol. 2009; 33(4):220–33. [PubMed: 19631083]
119. Vasung L, Huang H, Jovanov-Milosevic N, Pletikos M, Mori S, Kostovic I. Development of axonal pathways in the human fetal fronto-limbic brain: histochemical characterization and diffusion tensor imaging. J Anat. 2010; 217(4):400–17. [PubMed: 20609031]
120. Vasung L, Jovanov-Milosevic N, Pletikos M, Mori S, Judas M, Kostovic I. Prominent periventricular fiber system related to ganglionic eminence and striatum in the human fetal cerebrum. Brain Struct Funct. 2011; 215(3–4):237–53. [PubMed: 20953626]
121. Huang H, Jeon T, Sedmak G, Pletikos M, Vasung L, Xu X, Yarowsky P, Richards LJ, Kostovic I, Sestan N, Mori S. Coupling Diffusion Imaging with Histological and Gene Expression Analysis to Examine the Dynamics of Cortical Areas across the Fetal Period of Human Brain Development. Cereb Cortex. 2012
122. Zhan J, Dinov ID, Li J, Zhang Z, Hobel S, Shi Y, Lin X, Zamanyan A, Feng L, Teng G. Spatial-Temporal Atlas of Human Fetal Brain Development During the Early Second Trimester. Neuroimage. 2013
123. Moore RJ, Strachan B, Tyler DJ, Baker PN, Gowland PA. In vivo diffusion measurements as an indication of fetal lung maturation using echo planar imaging at 0. 5T. Magn Reson Med. 2001; 45(2):247–53. [PubMed: 11180432]
124. Balassy C, Kasprian G, Brugger PC, Csapo B, Weber M, Hormann M, Bankier A, Bammer R, Herold CJ, Prayer D. Diffusion-weighted MR imaging of the normal fetal lung. Eur Radiol. 2008; 18(4):700–6. [PubMed: 17924118]
125. Manganaro L, Perrone A, Sassi S, Fierro F, Savelli S, Di Maurizio M, Tomei A, Francioso A, La Barbera L, Giancotti A, Ballesio L. Diffusion-weighted MR imaging and apparent diffusion coefficient of the normal fetal lung: preliminary experience. Prenat Diagn. 2008; 28(8):745–8. [PubMed: 18567059]
126. Cannie M, Jani J, De Keyzer F, Roebben I, Dymarkowski S, Deprest J. Diffusion-weighted MRI in lungs of normal fetuses and those with congenital diaphragmatic hernia. Ultrasound Obstet Gynecol. 2009; 34(6):678–86. [PubMed: 19866446]
127. Kok RD, van den Bergh AJ, Heerschap A, Nijland R, van den Berg PP. Metabolic information from the human fetal brain obtained with proton magnetic resonance spectroscopy. Am J Obstet Gynecol. 2001; 185(5):1011–5. [PubMed: 11717623]
128. Kok RD, van den Berg PP, van den Bergh AJ, Nijland R, Heerschap A. Maturation of the human fetal brain as observed by 1H MR spectroscopy. Magn Reson Med. 2002; 48 (4):611–6. [PubMed: 12353277]
129. Kreis R, Hofmann L, Kuhlmann B, Boesch C, Bossi E, Huppi PS. Brain metabolite composition during early human brain development as measured by quantitative in vivo 1H magnetic resonance spectroscopy. Magn Reson Med. 2002; 48(6):949–58. [PubMed: 12465103]
130. Girard N, Fogliarini C, Viola A, Confort-Gouny S, Fur YL, Viout P, Chapon F, Levrier O, Cozzone P. MRS of normal and impaired fetal brain development. European journal of radiology. 2006; 57(2):217–225. [PubMed: 16387464]
131. Girard N, Gouny SC, Viola A, Le Fur Y, Viout P, Chaumoitre K, D'Ercole C, Gire C, Figarella-Branger D, Cozzone PJ. Assessment of normal fetal brain maturation in utero by proton magnetic resonance spectroscopy. Magn Reson Med. 2006; 56(4):768–75. [PubMed: 16964617]
132. Wolfberg AJ, Robinson JN, Mulkern R, Rybicki F, Du Plessis AJ. Identification of fetal cerebral lactate using magnetic resonance spectroscopy. Am J Obstet Gynecol. 2007; 196(1):e9–11. [PubMed: 17240215]

133. Brighina E, Bresolin N, Pardi G, Rango M. Human fetal brain chemistry as detected by proton magnetic resonance spectroscopy. Pediatr Neurol. 2009; 40(5):327–42. [PubMed: 19380068]

134. Story L, Damodaram MS, Allsop JM, McGuinness A, Wylezinska M, Kumar S, Rutherford MA. Proton magnetic resonance spectroscopy in the fetus. European Journal of Obstetrics & Gynecology and Reproductive Biology. 2011; 158(1):3–8. [PubMed: 20413207]

135. Story L, Damodaram MS, Allsop JM, McGuinness A, Patel A, Wylezinska M, Hagberg H, Kumar S, Rutherford MA. Brain metabolism in fetal intrauterine growth restriction: a proton magnetic resonance spectroscopy study. American journal of obstetrics and gynecology. 2011; 205(5):483. e1–483. e8. [PubMed: 21861969]

136. Yablonskiy DA, Neil JJ, Raichle ME, Ackerman JJ. Homonuclear J coupling effects in volume localized NMR spectroscopy: pitfalls and solutions. Magn Reson Med. 1998; 39(2):169–78. [PubMed: 9469698]

137. Fenton BW, Lin CS, Macedonia C, Schellinger D, Ascher S. The fetus at term: in utero volume-selected proton MR spectroscopy with a breath-hold technique--a feasibility study. Radiology. 2001; 219(2):563–6. [PubMed: 11323489]

138. Clifton MS, Joe BN, Zektzer AS, Kurhanewicz J, Vigneron DB, Coakley FV, Nobuhara KK, Swanson MG. Feasibility of magnetic resonance spectroscopy for evaluating fetal lung maturity. J Pediatr Surg. 2006; 41(4):768–73. [PubMed: 16567191]

139. Leithner K, Pörnbacher S, Assem-Hilger E, Krampl E, Ponocny-Seliger E, Prayer D. Psychological reactions in women undergoing fetal magnetic resonance imaging. Obstetrics & Gynecology. 2008; 111(2, Part 1):396–402. [PubMed: 18238978]

140. Murbach M, Neufeld E, Capstick M, Kainz W, Brunner DO, Samaras T, Pruessmann KP, Kuster N. Thermal Tissue Damage Model Analyzed for Different Whole-Body SAR and Scan Durations for Standard MR Body Coils. Magn Reson Med. 2013

141. Neufeld E, Gosselin MC, Murbach M, Christ A, Cabot E, Kuster N. Analysis of the local worst-case SAR exposure caused by an MRI multi-transmit body coil in anatomical models of the human body. Phys Med Biol. 2011; 56(15):4649–59. [PubMed: 21734334]

142. Merkle EM, Dale BM. Abdominal MRI at 3. 0 T: the basics revisited. AJR Am J Roentgenol. 2006; 186(6):1524–32. [PubMed: 16714640]

143. Bernstein MA, Huston J 3rd, Ward HA. Imaging artifacts at 3. 0T. J Magn Reson Imaging. 2006; 24(4):735–46. [PubMed: 16958057]

144. Victoria T, Jaramillo D, Roberts TP, Zarnow D, Johnson AM, Delgado J, Rubesova E, Vossough A. Fetal magnetic resonance imaging: jumping from 1. 5 to 3 tesla (preliminary experience). Pediatr Radiol. 2014; 44(4):376–86. [PubMed: 24671739]

145. Heerschap A, Kok RD, van den Berg PP. Antenatal proton MR spectroscopy of the human brain in vivo. Child's Nervous System. 2003; 19(7–8):418–421.

146. Malamateniou C, Malik SJ, Counsell SJ, Allsop JM, McGuinness AK, Hayat T, Broadhouse K, Nunes RG, Ederies AM, Hajnal JV. Rutherford MA, Motion-compensation techniques in neonatal and fetal MR imaging. AJNR Am J Neuroradiol. 2013; 34(6):1124–36. [PubMed: 22576885]

147. Klessen C, Asbach P, Kroencke TJ, Fischer T, Warmuth C, Stemmer A, Hamm B, Taupitz M. Magnetic resonance imaging of the upper abdomen using a free-breathing T2-weighted turbo spin echo sequence with navigator triggered prospective acquisition correction. J Magn Reson Imaging. 2005; 21(5):576–82. [PubMed: 15834908]

148. Cetin I, Barberis B, Brusati V, Brighina E, Mandia L, Arighi A, Radaelli T, Biondetti P, Bresolin N, Pardi G. Lactate detection in the brain of growth-restricted fetuses with magnetic resonance spectroscopy. American journal of obstetrics and gynecology. 2011; 205(4):350. e1–350. e7. [PubMed: 21861968]

149. Rousseau F, Glenn OA, Iordanova B, Rodriguez-Carranza C, Vigneron DB, Barkovich JA, Studholme C. Registration-based approach for reconstruction of high-resolution in utero fetal MR brain images. Acad Radiol. 2006; 13(9):1072–81. [PubMed: 16935719]

150. Jiang S, Xue H, Glover A, Rutherford M, Rueckert D, Hajnal JV. MRI of moving subjects using multislice snapshot images with volume reconstruction (SVR): application to fetal, neonatal, and adult brain studies. IEEE Trans Med Imaging. 2007; 26(7):967–80. [PubMed: 17649910]

151. Gholipour A, Estroff JA, Warfield SK. Robust super-resolution volume reconstruction from slice acquisitions: application to fetal brain MRI. IEEE Trans Med Imaging. 2010; 29(10):1739–58. [PubMed: 20529730]

152. Kim K, Habas PA, Rousseau F, Glenn OA, Barkovich AJ, Studholme C. Intersection based motion correction of multislice MRI for 3-D in utero fetal brain image formation. IEEE Trans Med Imaging. 2010; 29(1):146–58. [PubMed: 19744911]

153. Kuklisova-Murgasova M, Quaghebeur G, Rutherford MA, Hajnal JV, Schnabel JA. Reconstruction of fetal brain MRI with intensity matching and complete outlier removal. Med Image Anal. 2012; 16(8):1550–64. [PubMed: 22939612]

154. Schopf V, Kasprian G, Brugger P, Prayer D. Watching the fetal brain at 'rest'. International Journal of Developmental Neuroscience. 2012; 30(1):11–17. [PubMed: 22044604]

155. Seshamani S, Cheng X, Fogtmann M, Thomason ME, Studholme C. A method for handling intensity inhomogenieties in fMRI sequences of moving anatomy of the early developing brain. Med Image Anal. 2014; 18(2):285–300. [PubMed: 24317121]

156. Ferrazzi G, Kuklisova Murgasova M, Arichi T, Malamateniou C, Fox MJ, Makropoulos A, Allsop J, Rutherford M, Malik S, Aljabar P, Hajnal JV. Resting State fMRI in the moving fetus: a robust framework for motion, bias field and spin history correction. Neuroimage. 2014; 101:555–68. [PubMed: 25008959]

157. Corbett-Detig J, Habas PA, Scott JA, Kim K, Rajagopalan V, McQuillen PS, Barkovich AJ, Glenn OA, Studholme C. 3D global and regional patterns of human fetal subplate growth determined in utero. Brain Struct Funct. 2011; 215(3–4):255–63. [PubMed: 21046152]

158. Jacob FD, Habas PA, Kim K, Corbett-Detig J, Xu D, Studholme C, Glenn OA. Fetal hippocampal development: analysis by magnetic resonance imaging volumetry. Pediatr Res. 2011; 69(5 Pt 1): 425–9. [PubMed: 21270675]

159. Rajagopalan V, Scott J, Habas PA, Kim K, Corbett-Detig J, Rousseau F, Barkovich AJ, Glenn OA, Studholme C. Local tissue growth patterns underlying normal fetal human brain gyrification quantified in utero. J Neurosci. 2011; 31(8):2878–87. [PubMed: 21414909]

160. Rajagopalan V, Scott J, Habas PA, Kim K, Rousseau F, Glenn OA, Barkovich AJ, Studholme C. Mapping directionality specific volume changes using tensor based morphometry: an application to the study of gyrogenesis and lateralization of the human fetal brain. Neuroimage. 2012; 63(2): 947–58. [PubMed: 22503938]

161. Gholipour A, Akhondi-Asl A, Estroff JA, Warfield SK. Multi-atlas multi-shape segmentation of fetal brain MRI for volumetric and morphometric analysis of ventriculomegaly. Neuroimage. 2012; 60(3):1819–31. [PubMed: 22500924]

162. Clouchoux C, Kudelski D, Gholipour A, Warfield SK, Viseur S, Bouyssi-Kobar M, Mari JL, Evans AC, du Plessis AJ, Limperopoulos C. Quantitative in vivo MRI measurement of cortical development in the fetus. Brain Struct Funct. 2012; 217(1):127–39. [PubMed: 21562906]

163. Clouchoux C, du Plessis AJ, Bouyssi-Kobar M, Tworetzky W, McElhinney DB, Brown DW, Gholipour A, Kudelski D, Warfield SK, McCarter RJ, Robertson RL Jr, Evans AC, Newburger JW, Limperopoulos C. Delayed Cortical Development in Fetuses with Complex Congenital Heart Disease. Cereb Cortex. 2012

164. Scott JA, Habas PA, Kim K, Rajagopalan V, Hamzelou KS, Corbett-Detig JM, Barkovich AJ, Glenn OA, Studholme C. Growth trajectories of the human fetal brain tissues estimated from 3D reconstructed in utero MRI. Int J Dev Neurosci. 2011; 29(5):529–36. [PubMed: 21530634]

165. Scott JA, Hamzelou KS, Rajagopalan V, Habas PA, Kim K, Barkovich AJ, Glenn OA, Studholme C. 3D morphometric analysis of human fetal cerebellar development. Cerebellum. 2012; 11(3): 761–70. [PubMed: 22198870]

166. Scott JA, Habas PA, Rajagopalan V, Kim K, Barkovich AJ, Glenn OA, Studholme C. Volumetric and surface-based 3D MRI analyses of fetal isolated mild ventriculomegaly: brain morphometry in ventriculomegaly. Brain Struct Funct. 2013; 218(3):645–55. [PubMed: 22547094]

167. Vatansever D, Kyriakopoulou V, Allsop JM, Fox M, Chew A, Hajnal JV, Rutherford MA. Multidimensional analysis of fetal posterior fossa in health and disease. Cerebellum. 2013; 12(5): 632–44. [PubMed: 23553467]

168. Cheng X, Wilm J, Seshamani S, Fogtmann M, Kroenke C, Studholme C. Adapting parcellation schemes to study fetal brain connectivity in serial imaging studies. Conf Proc IEEE Eng Med Biol Soc. 2013; 2013:73–6. [PubMed: 24109627]

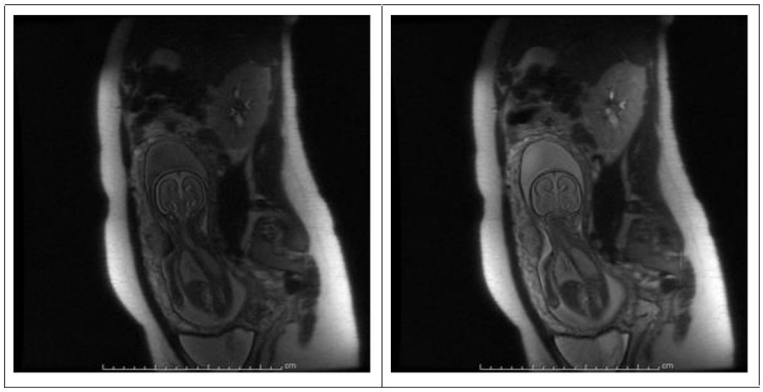

Figure 1.

Left: SST2W image acquired as one of 19 images in a stack of slices acquired in approximately 15 s total scan time with less than 1 second between sequential slice acquisitions. Right: SST2W image with identical window settings and sequence parameters but acquired as a single acquisition with no slices interrogated on either side. Note that signal from the amniotic fluid is nearly twice as bright and the brain signal approximately 1.4 × brighter in the latter image while both maternal fat and noise signals are the same in both images. This is an example of how rapid sequential slice sampling (left), though critical to avoid inter-sequence fetal movement, can lead to direct (amniotic fluid saturation and convective motion) and indirect (magnetization transfer) saturation effects which can detract from image signal-to-noise. These images were generated on a GE 1.5 T scanner with a 256×384 image matrix, half-Fourier sampling, 4 mm slice thickness, 34×44 cm^2 FOV and an effective echo time of 78 ms. The fetus in this exam had agenesis of corpus callosum.

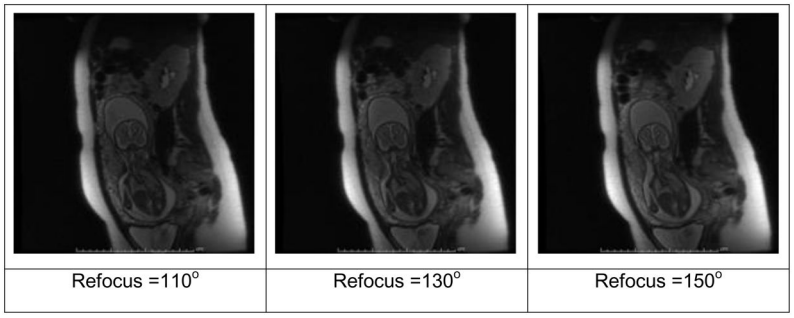

Figure 2.

SST2W images of the fetus shown in Figure 1 with different refocusing flip angles of (left to right) 110°, 130° and 150°. The images are windowed identically and a small increase in overall tissue signal is seen with increasing refocusing flip angle.

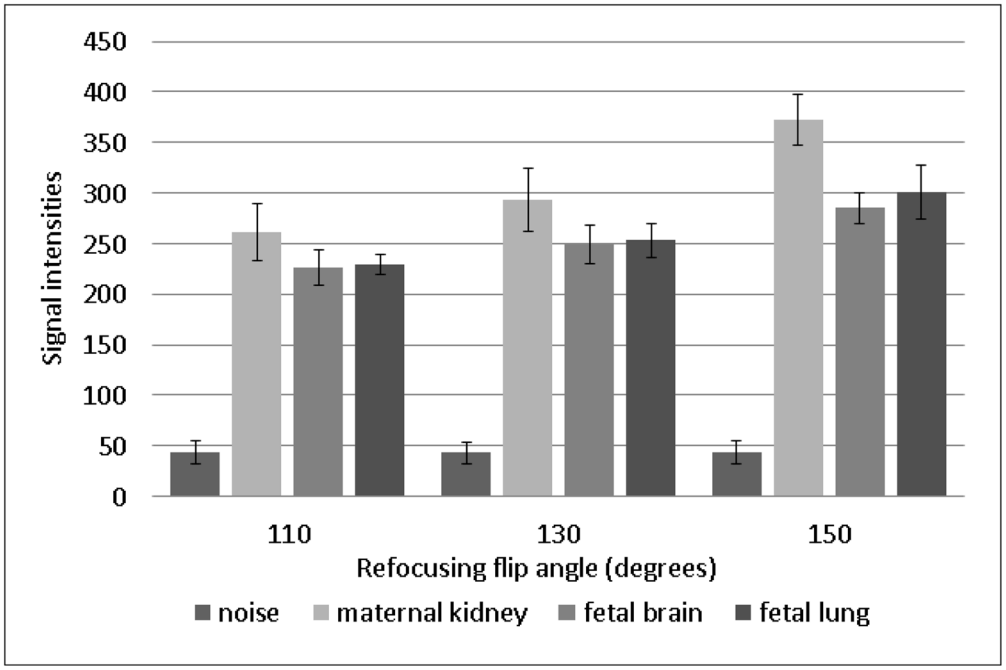

Figure 3.

Measurements of signal from maternal kidney, fetal brain, fetal lung and noise from an air ROI are shown as a function of flip angle for the SST2W images of figure 2. The increase in signal depends on the tissue type and is a complex function of both transverse and longitudinal relaxation times as well as magnetization transfer properties.

Figure 4.

An SST1W image as acquired with the inversion recovery technique using a relatively long inversion time of 2000 ms. The image matrix (phase × frequency) of 192×256 meant that 112 echoes were employed with an echo spacing on the order of 4 ms. To reduce T2-weighting, early echoes were encoded with the low phase encodes to achieve an effective echo time (ETE) of 35 ms, leaving the higher phase encode steps with diminished signal intensity, resulting in an overall blurry caste to the image. CSF is dark and fat is bright with this inversion time, as expected for T1-contrast, though the use of magnitude reconstructions currently in-place reduces the dynamic range of the T1-contrast and can lead to ambiguity as to which side of the T1 null point tissue T1's actually reside (see next figure).

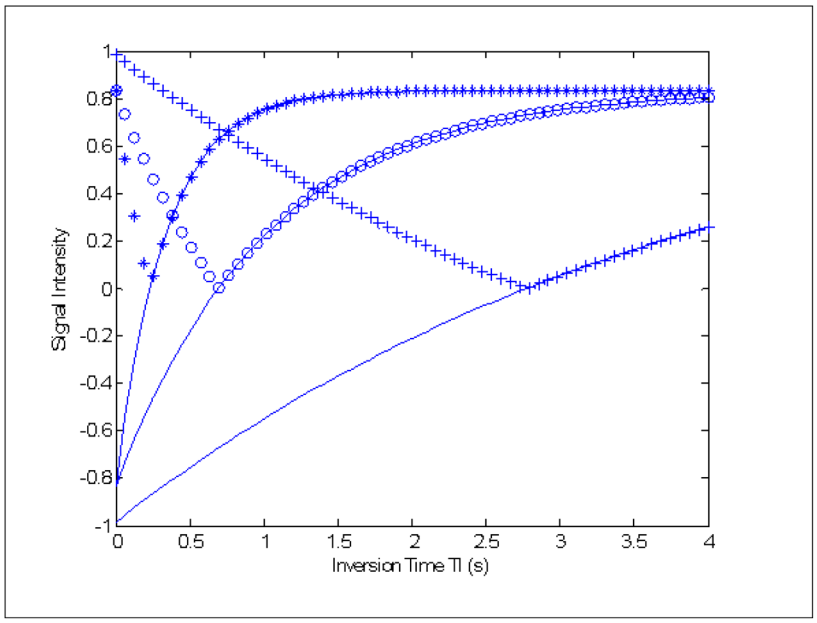

Figure 5.

Rationale for an inversion time TI of 2 s for SST1W fetal imaging. Magnitude signal intensities as a function of inversion time for three simulated tissues fat (*'s), fetal brain parenchyma (o's), and cerebrospinal fluid (+'s). The R1 and R2 values for fat, brain and CSF used were 3 and 6 s^{-1}, 1 and 6 s^{-1}, and 3 and 6 s^{-1}, respectively with the solid lines showing the curves generated if (more difficult) phase reconstructions rather than magnitude reconstructions were employed. Note that at a TI of 2 s, fat is bright, brain parenchyma intermediate, and CSF dark, as expected for contrast mimicking a classic short TR/short TE spin echo experiment. Note that if phase reconstructions were available, all three tissues would have unique signal intensities at any TI but due to magnitude reconstructions, cross-over points exist where, for example, CSF and brain parenchyma would share the same signal intensity at TI ~ 1.35 s.

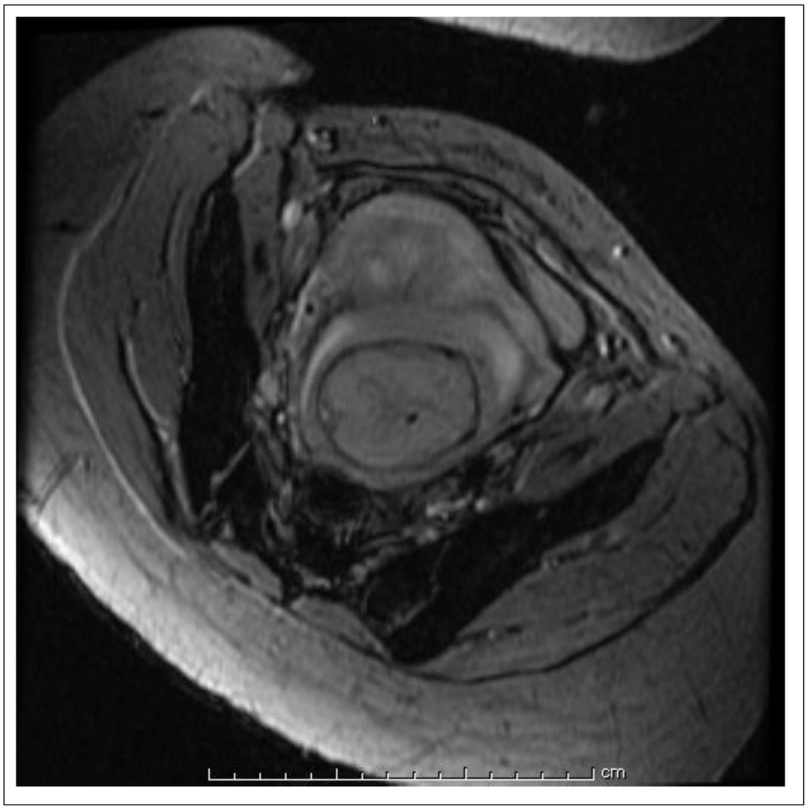

Figure 6.

T2* weighted gradient echo sequence acquired as one in a 4 slice stack in 23 seconds using TR/TE/FA = 150/25/20, a 4 mm slice thickness, 1 mm gap, and a 256×128 (frequency × phase) matrix with a 46×30 cm^2 FOV. Note the periventricular hypointense lesion suspected to be blood (hemorrhagic lesion) with a short T2*. This lesion was subtle or not appreciated on SST2W, T1-weighted gradient echo, and SSFP sequences applied in this study.

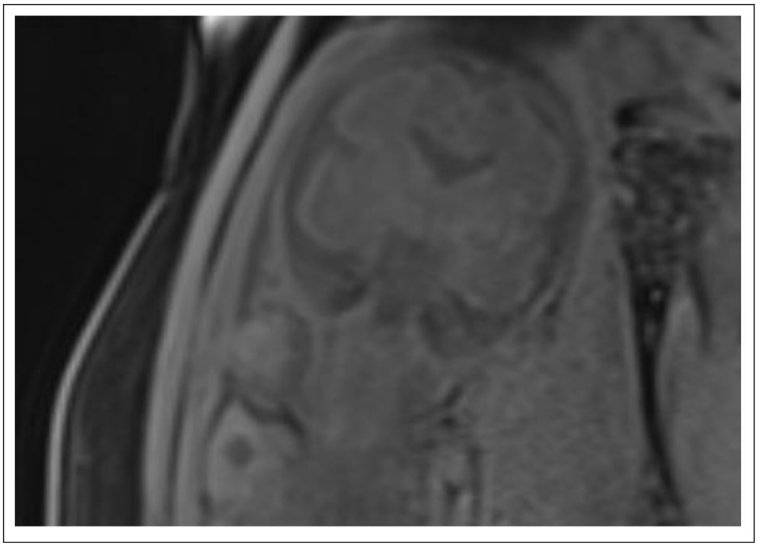

Figure 7.

A VIBE scan used for T1-weighted imaging of a 30 week and 4 day GA fetus acquired on a Siemens Skyra 3T scanner with an eight channel body coil. The parameters used in this scan were TR/TE=3.64/1.28 ms, FA=9°, ETL=1, number of averages=1, and slice thickness=2 mm. The total acquisition time was 9 seconds. Note that like other 3D sequences, VIBE is very sensitive to motion, thus good-quality images may only be achieved under conditions of minimal fetal and maternal motion.

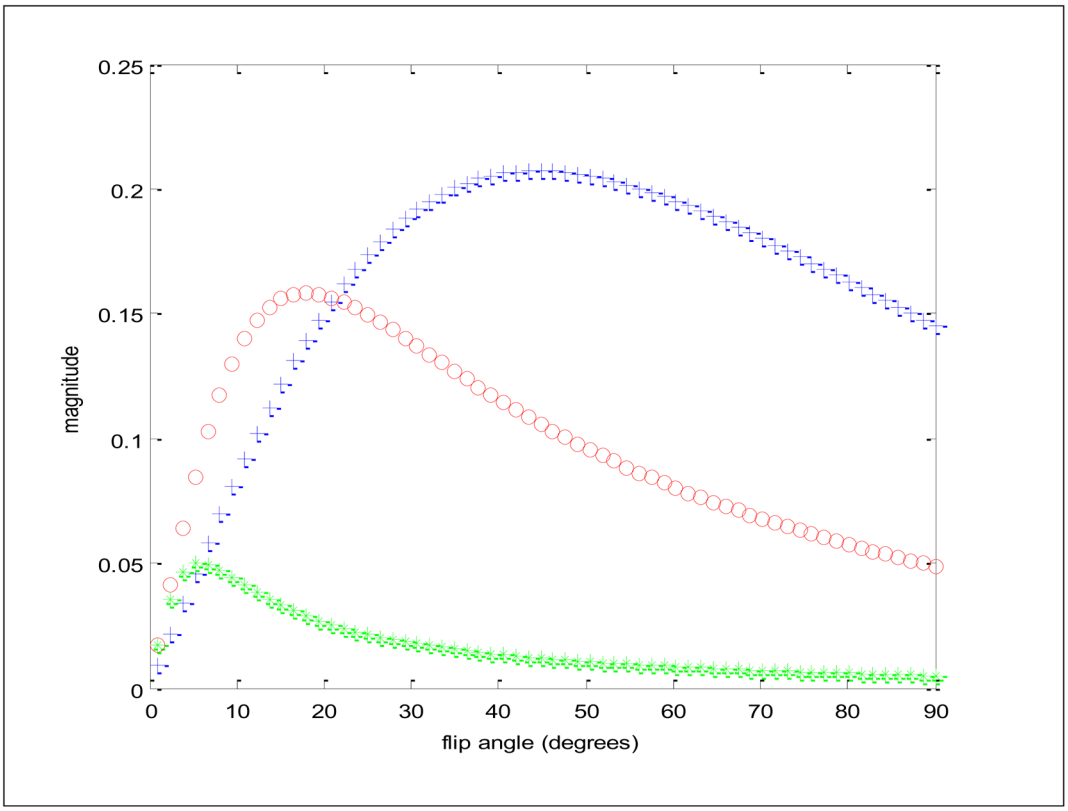

Figure 8.

How unspoiled gradient echo sequences dramatically outperform spoiled gradient echo sequences in SNR/unit time is exemplified here by plotting the magnitude signal vs. flip angle for a tissue like fetal brain parenchyma with longitudinal and transverse relaxations rates $R_1 = 1\ s^{-1}$ and $R_2 = 6\ s^{-1}$, respectively. All curves display the steady state signal immediately after each pulse from a repetitive train of pulses with the crosses (+) and star (*) plots generated with unspoiled and spoiled gradient echo sequences, respectively and with a repetition time TR of 5 ms between pulses. Note how the unspoiled sequence yields some 4 times large signal at a substantially higher flip angle. The plot displayed with circles (o) is for a spoiled gradient echo sequence in which the TR was increased to 50 ms, and so would acquire images 10x slower than either of the other two settings. Note even with the slowdown of a factor of 10 the unspoiled gradient echo sequence still yields substantially higher signal than the spoiled gradient echo sequence (at their respective optimal flip angles) by approximately 0.2/0.15 or 25 %.

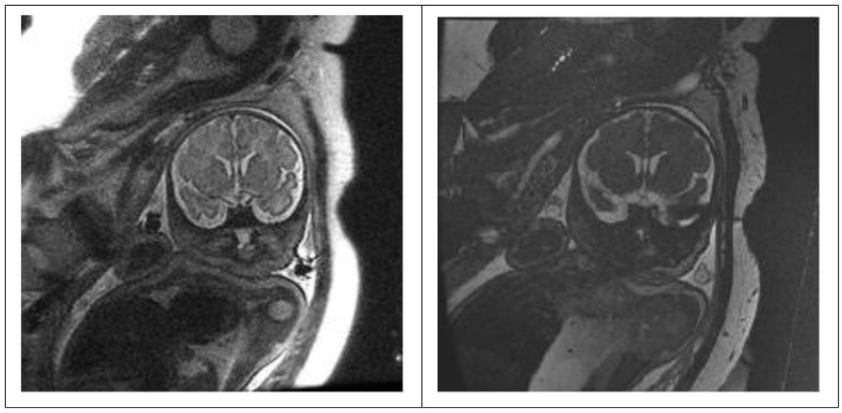

Figure 9.

Comparison of SST2W image (left, TR/TE = 4500/100 with 3 mm thick slice) with an unspoiled gradient echo image (right, TR/TE/FA = 4.8/2.1/75 with a 4 mm thick slice and 2 NEX). Note brain SNR's are approximately 4 and 2 for the SST2W and SSFP images, respectively. The latter image, however, could be repeated without loss of SNR over and over again at rapid (~ 1 s intervals) to monitor fetal motion while this could not be done at such high rates with SST2W imaging without tissue saturation and significant image degradation.

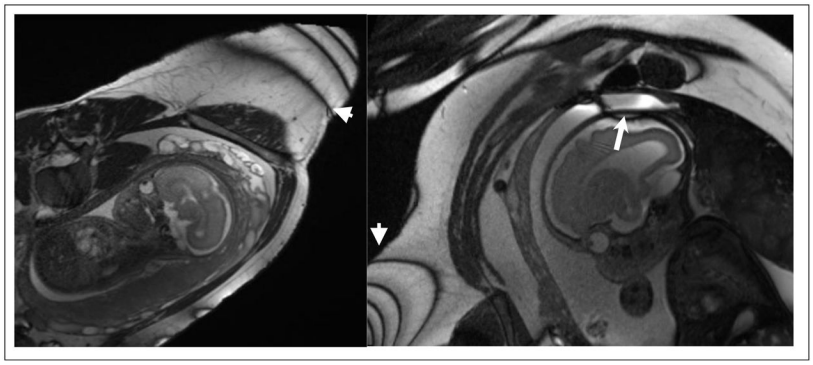

Figure 10.

Banding artifacts in a SSFP scan with TR/TE = 4.4/1.9ms, matrix size of 320×320, 2 mm slice thickness, FOV=30×37 cm^2, FA=69°, and 19 slices acquired on a 3T scanner; the bands are towards the outer limits of the FOV and well-away from the fetus (arrowheads), but other, subtler, bands attributed to frequency shifts in maternal bowel and closer to the fetus may also be present (arrow).

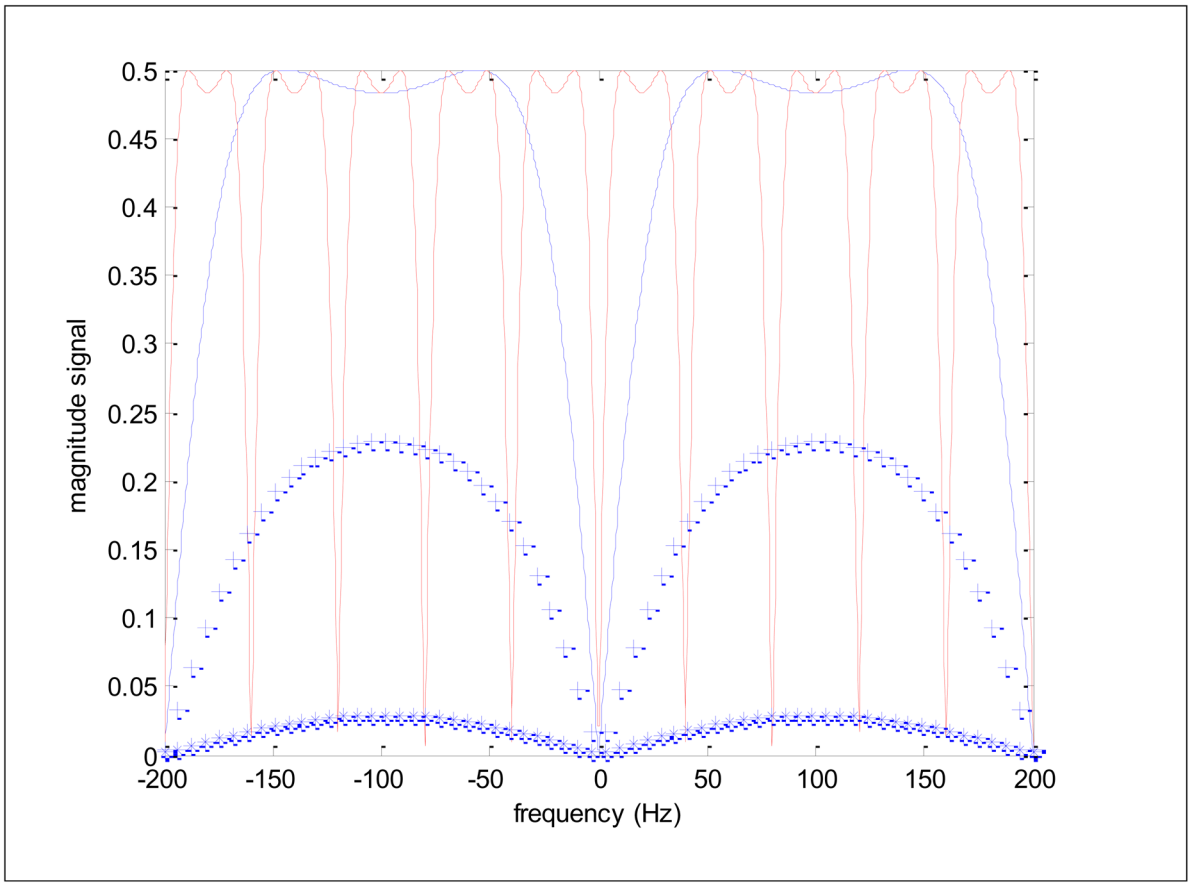

Figure 11.

Magnitude SSFP signals as a function of frequency for a tissue with T1 = T2 = 3 s and for repetition times TR of 5 ms (solid blue) and 25 ms (solid red) and with a flip angle of 75° with TE = TR/2 in both cases. Fetal brain parenchyma, with T1 = 1 s and T2 = 0.25 s (blue +'s) and muscle tissue with T1 = 1.5 s and T2 = 0.035 s (blue *'s) are also simulated for the TR/TE = 5 ms/2.5 ms case and show decreased signal approximated by the ratios of T1/T2.

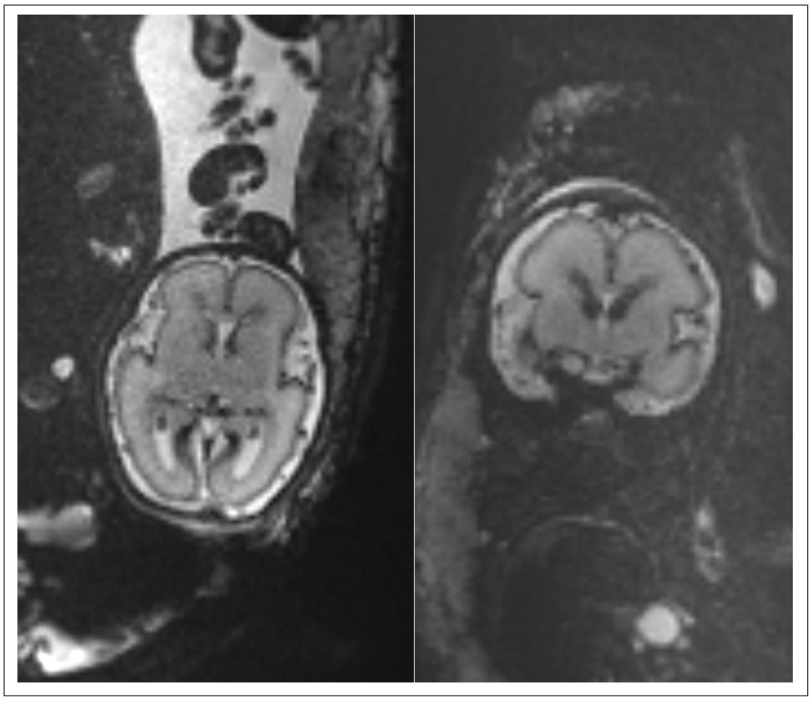

Figure 12.

Axial and coronal EPI scans of a 26 week GA fetus acquired on a Siemens Skyra 3T scanner with iPAT2 parallel imaging, TR/TE = 6620/80 ms, ETL = 119, number of averages 1, and slice thickness of 2 mm. Note that EPI is very rapid but is frequently affected by geometric distortion and motion-induced signal intensity artifacts.

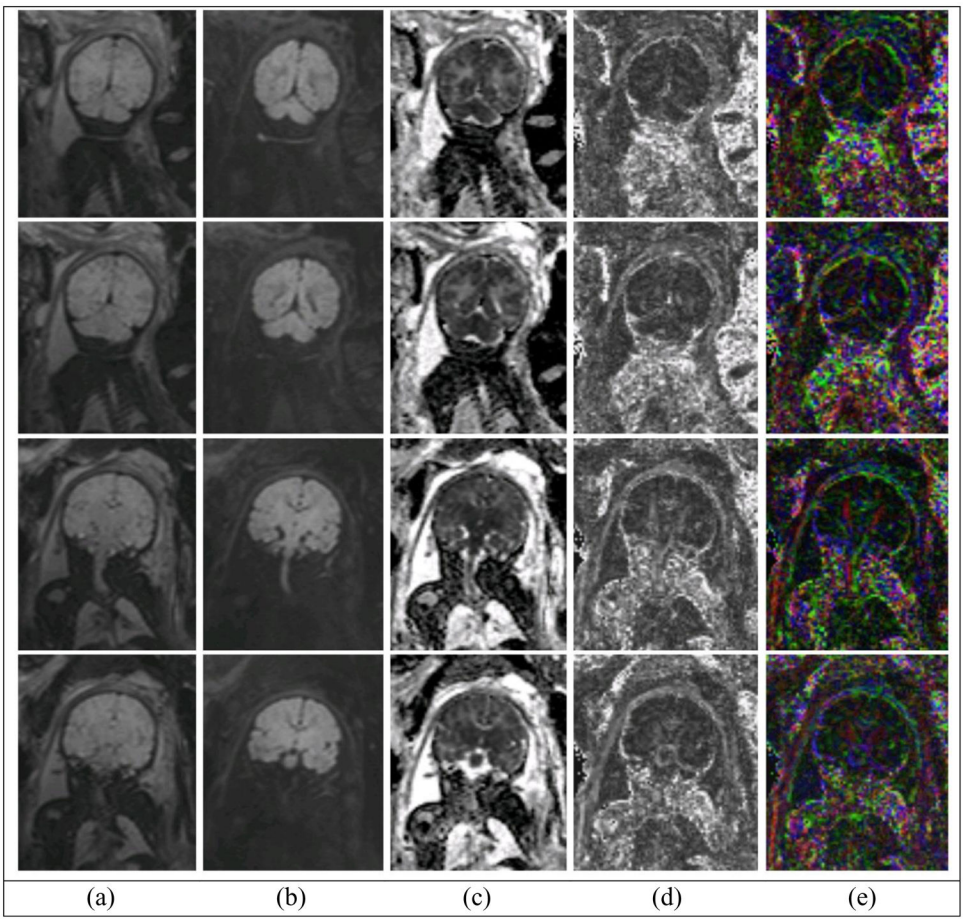

Figure 13.

Coronal DWI slices of a 39 week gestation age fetus acquired on a Philips Achieva 1.5 T scanner (DWI with high b value of 500 s/mm^2 and 6 gradient directions); (a) b=0 image, (b) DWI image, (c) ADC, (d) FA, and (e) color FA. FA and color FA maps are apparently more sensitive to motion as compared to the ADC map. Motion correction is critical in the analysis of fetal DWI scans.

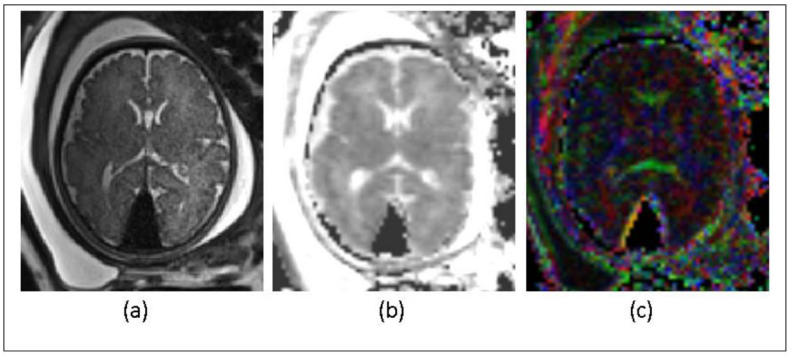

Figure 14.

(a): Axial SST2W image of 36-week gestation fetus with dural sinus fistula. (b) and (c): ADC and color FA maps of the comparable slice obtained from diffusion weighted imaging (DWI). Images were acquired with a 3 T Siemens Skyra scanner. The SST2W images were 3 mm thick, no gap, and with an in-plane resolution of 1×1 mm^2. The DWI scan was acquired with TR/TE=5500/68 ms, echo train length of 47, 30 slices with slice thickness of 3 mm, and in-plane resolution of 2 mm^2, with two b=0 images and 12 gradient directions with b=500 s/mm^2. The images acquired for this fetus showed enlargement of the torcular and transverse sinuses with dural arteriovenous fistula/malformation, but with no evidence of brain injury. The ADC and color FA maps also confirmed intact development of corpus callosum and no evidence of white matter injury, which led to good neurodevelopment prognosis in this fetus. This was compatible with postnatal imaging and outcomes.

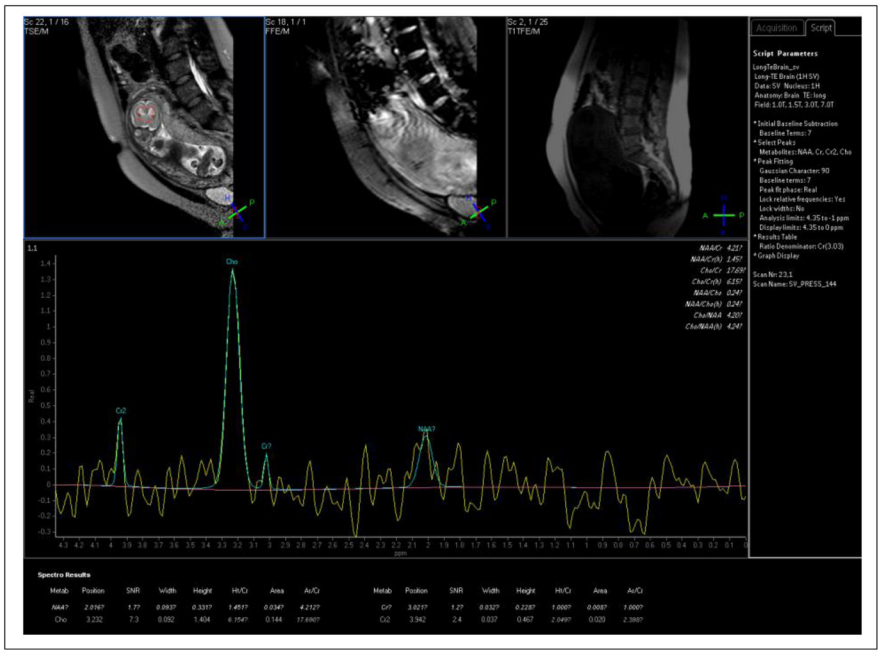

Figure 15.

Brain spectrum from 20 week gestational age fetus (TR/TE = 1500/144 ms/ms, 64 signal averages) showing prominent choline resonance at 3.2 ppm with only a small signal from N-acetyl aspartate (NAA) at 2.0 ppm. Spectrum acquired using a 1.5 T Philips scanner with a 4-element array body coil.

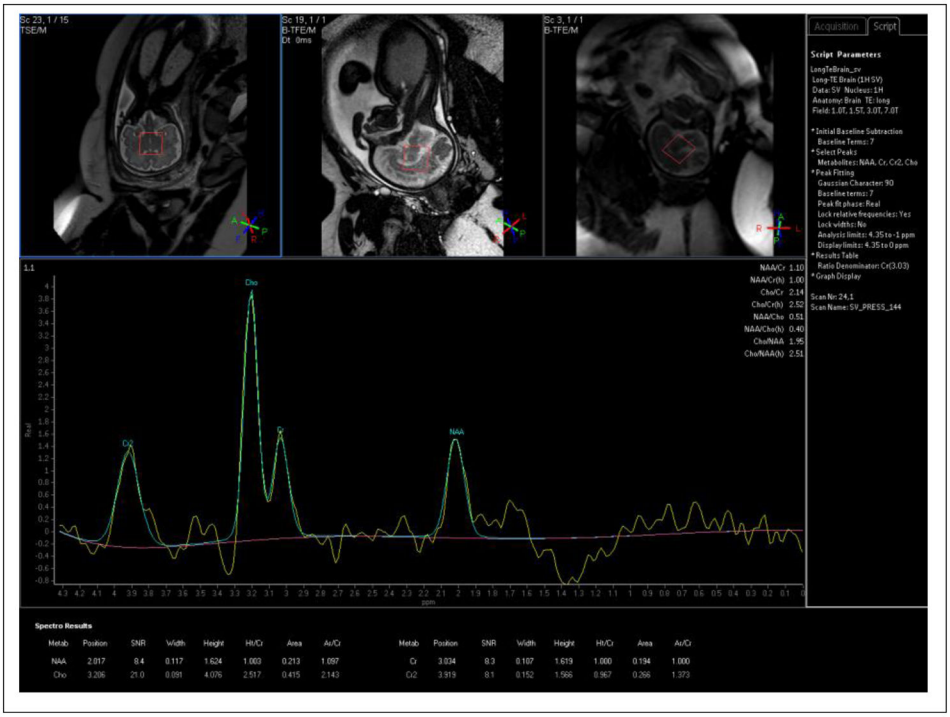

Figure 16.

Brain spectrum (TR/TE= 1500/144 ms/ms. 64 signal averages) from 33 week gestation fetus showing prominent resonances from choline, creatine and NAA with, perhaps, an inverted lactate doublet around 1.1 ppm. Though choline is still the prominent resonance, the creatine and NAA peaks, largely unobservable in the 20 week GA fetus, are now quantifiable. Spectrum acquired using a 1.5 T Philips scanner with a 4-element array body coil.

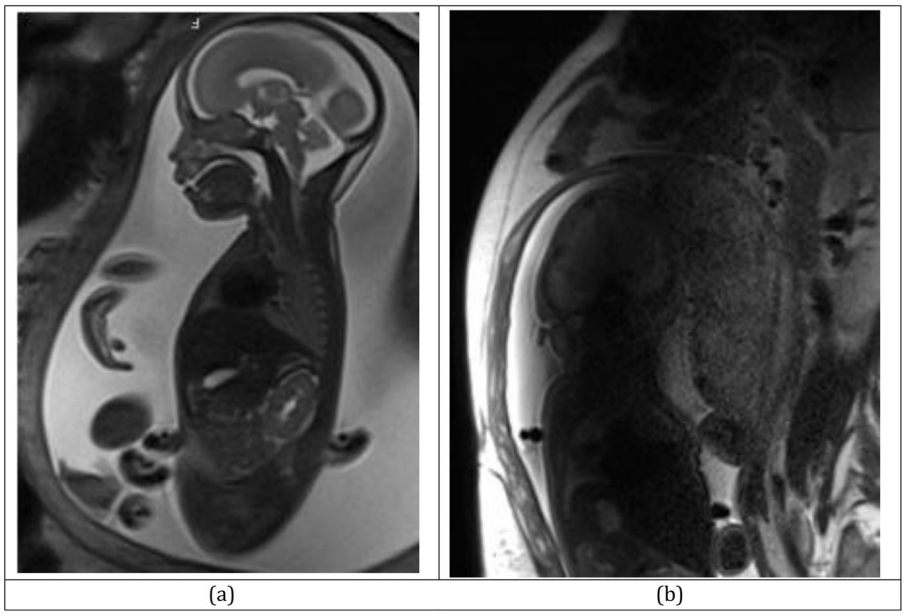

Figure 17.

SST2W MRI scan on a Siemens Skyra 3T scanner; with TR=2s, TE=121ms, ETL=109, FA=153, number of averages=1, Slice thickness: 3mm, Acquisition matrix: 256×256: (a) high-quality SST2W fetal MRI acquired at 3 Tesla, (b) Fetal MRI degraded by RF penetration and conductivity artifact, which occasionally degrades the fetal MRI scans at 3T. A multi-transmit system may reduce this artifact by generating a more homogeneous B_1 field across the FOV. A dielectric pad may be used to do the same.

Table 1

How we do it: parameters of our fetal MRI protocol as implemented on a 3T Scanner (TR: repetition time in ms, TE: echo time in ms, FA: flip angle in degrees, BW: bandwidth in Hz/pixel, spacing and slice thickness in mm, ETL: echo train length, and PF: partial Fourier acquisition). All sequences utilize a combination of body and spine coils. In all sequences parallel imaging with GRAPPA (an iPAT factor of 2) is used. The SST2W, SST1W, and SSFP are examined in all three planes and are repeated multiple times in each plane. These sequences are performed with 2 or 4 concatenations to minimize slice cross talk and spin history artifacts. To accelerate imaging, autoprescan is only performed in the first scan of each type of sequence and is omitted in the subsequent scans. The sequences are sorted and performed based on their relative importance; at least one third of a session but typically about half of a session is dedicated to SST2W scans, about one third is spent on gradient echo sequences (i.e. SSFP and SPGR), and the rest is spent on other sequences; however, this varies based on the clinical indication and the region of interest (ROI). The field of view (FOV) is variable between 26 to 42 cm depending on the sequence, gestation age, and the size of the ROI. Phase oversampling of up to 50% may be used to avoid wrap-around artifacts when the FOV and matrix size are kept fixed to maintain specific image spacing. The number of averages (NEX) is often set to 1 to avoid motion degradation; however if motion is negligible a 2 NEX may be used to achieve higher SNR in some sequences. We use an inversion recovery time of 2000 ms in SST1W imaging and a maximum b factor of 500 s/mm^2 in DWI scans.

Sequence/parameter	**TR**	**TE**	**FA**	**BW**	**Spacing**	**Slice**	**ETL**	**PF**	**TA**
Unit	**ms**	**ms**	**deg.**	**Hz/px**	**mm**	**mm**	**---**	**---**	**seconds**
SPGR (3 plane localizer)	15	6	30°	130	0.8	10	1	Off	~10
SST2W (T2 3 planes)	1400	102	160°	698	1.0	2.0	120	5/8	30–60
SST1W (T1 IR 3 planes)	1240	61	135°	514	1.3	3.0	74	4/8	30–60
SSFP (GRE 3 planes)	4.23	1.81	75°	601	0.9	3.0	1	Off	20–50
SSFP (Cinematographic)	4.73	2.37	70°	566	0.9	4.0	1	Off	40–120
SPGR (T2* 3 planes)	150	25	20°	380	2.2	5.0	1	6/8	20–30
EPI2D	6000	80	90°	1358	2.0	3.0	119	Off	10–30
DWI	4200	62	---	1775	2.0	3.0	62	6/8	40–100
VIBE (T1 3D SPGR)	3.64	1.28	9°	450	1.3	2.0	1	7/8	~10